THE CROSS-SECTIONAL SHAPE OF THE DISTANT GEOMAGNETIC TAIL

L. C. Evans

Internal Report # 26

Space Radiation Laboratory
California Institute of Technology
Pasadena, California 91109

August, 1971

THE CROSS-SECTIONAL SHAPE OF THE DISTANT GEOMAGNETIC TAIL

L. C. Evans

August 1971

It has been suggested that the shape of the distant geomagnetic tail may be of critical importance in understanding the mechanism of particle access onto open geomagnetic field lines (Michel and Dessler, 1970). Specifically, the anisotropic pressure exerted on the geomagnetic tail by the interplanetary magnetic field, which has been distorted by the presence of the tail, can be expected to tend to "flatten" the tail (i.e., the cross section of the tail should show a pronounced ellipticity some distance from the Earth). The magnitude of this ellipticity assumed by Michel and Dessler (2000 R_E major axis and 10 R_E minor axis at $\sim 10^4$ R_E behind the Earth) led them to postulate that the tail becomes filamentary at large distances. This, in turn, led to the postulation of a different mechanism of access onto open geomagnetic field lines for high energy protons than for low energy protons. Furthermore, the definition of the distinction between "high" and "low" energies is apparently critically dependent upon the magnitude of the ellipticity. Also, since the method by which particles gain rapid access to the open field lines is dependent upon the filamentary nature of the geomagnetic tail, the position of the beginning of this filamentary region defines the position of the beginning of the region of rapid access. A more careful investigation of the shape of the distant geomagnetic tail would seem to be of critical importance to the access model proposed by Michel and Dessler. The purpose of this study is such an investigation, in view of the current infeasibility of a direct magnetometer mapping of the configuration of the distant tail field.

The present study was predicated on the following assumptions:

1. The parameters and configurations of the solar wind, interplanetary magnetic field, and geomagnetic tail are uniform (time-independent).

2. The cross-sectional shape of the geomagnetic tail is always strictly elliptical.

3. The longitudinal axis of the tail ($-x_{SM}$) is parallel to the average solar wind velocity.

4. The boundaries of the geomagnetic tail are everywhere defined by the position of the magnetopause.

5. The position of the magnetopause represents an equilibrium as defined by the balancing of the several forces acting on the magnetopause (see below for a discussion of these pressures).

6. The surface defined by the magnetopause is continuous.

7. Instabilities and waves in the magnetopause do not, to a first approximation, affect the overall shape of the tail.

8. No significant merging takes place between the interplanetary magnetic field and the geomagnetic field.

Assumptions 1, 2 and 7 are the most critical and the most questionable, but all reduce the computational complexity of the problem considerably. The second is a necessary consequence of a conformal transformation used, and cannot be relaxed in the context of this study; tests have, however, shown it to be reasonable to a first approximation. The first assumption can be relaxed merely by assuming that the interplanetary or geomagnetic parameters vary as a function of position in a non-uniform manner. Although this would be simple enough to do in the context of this study, it has not been done and probably represents an unwarranted degree of complexity. The seventh assumption could be relaxed if more were known about the modes of instabilities and waves in the magnetopause and if the effects of these instabilities and

waves could be translated into equivalent "pressures". This again probably represents an unwarranted degree of complexity in the context of this study.

The following pressures (and no others) are assumed to affect the equilibrium position of the magnetopause:

p_1 - Isotropic pressure of the solar wind plasma. Since the axis of the geomagnetic tail is assumed to be parallel to the solar wind velocity, this pressure will be exerted perpendicularly to the surface of the tail and will be independent of the cross sectional shape of the tail.

p_2 - Pressure from the component of the interplanetary magnetic field parallel to the solar wind velocity. This pressure will also be independent of the cross sectional shape of the tail.

p_3 - Pressure from the component of the interplanetary magnetic field perpendicular to the solar wind velocity. It is this pressure which tends to "flatten" the tail. This component is assumed to be parallel to the ecliptic plane far from the geomagnetic tail.

p_4 - Isotropic pressure from the plasma in the geomagnetic tail. Little is known about the detailed distribution of this plasma, and it is probably safe to assume an initially isotropic distribution. This pressure will depend on angular position within the tail only to the extent of any compressional or expansional effects as the shape changes.

p_5 - Pressure from the geomagnetic field in the tail, which is assumed to be pulled into a spiral configuration due to the rotation of the Earth (Dessler and Juday, 1965).

p_6 - Pressure exerted on the surface of the tail by the solar wind corresponding to the pressure exerted by a supersonic fluid on a surface over which it is flowing.

$\hat{e}_n$

We must first determine an expression for the unit normal to the tail surface through any arbitrary point (x_o, y_o, z_o). To do this we must first obtain expressions for the tangent to each of two curves through the point (x_o, y_o, z_o) and along the surface (see figure 1). Since assumption 2 (that all cross sections are elliptical) is necessary in order to transform the anisotropic pressures, a natural choice for one of the curves is the intersection of the surface and the plane $x = x_o$, which is given by

C1:
$$\begin{aligned} x &= x_o \\ y &= R_o \cos\theta \\ z &= \alpha_o R_o \sin\theta \\ \alpha_o &= \alpha(x_o) \\ R_o &= R(x_o) \end{aligned} \tag{1}$$

See figure 2. From Eq. (1) the tangent can be easily found to be

$$\vec{T}_1 = \frac{-\sin\theta\ \hat{e}_y + \alpha\cos\theta\ \hat{e}_z}{(\sin^2\theta + \alpha^2\cos^2\theta)^{1/2}} \tag{2}$$

The other curve will be the intersection of the surface with the half-plane $\theta = \theta_o$, which can be expanded in a Taylor series around (x_o, y_o, z_o):

C2:
$$\begin{aligned} x &= x_o + \delta \\ y &= y_o + \delta \frac{dy}{dx}\Big|_{x_o} + \frac{\delta^2}{2} \frac{d^2y}{dx^2}\Big|_{x_o} + \cdots \\ z &= z_o + \delta \frac{dz}{dx}\Big|_{x_o} + \frac{\delta^2}{2} \frac{d^2z}{dx^2}\Big|_{x_o} + \cdots \end{aligned} \tag{3}$$

which are

$$x = x_o + \delta$$

$$y = y_o + \delta R'(x)\cos\theta + \frac{\delta^2}{2}R''(x)\cos\theta + \ldots \tag{4}$$

$$z = z_o + \delta(R'(x)\alpha(x) + \alpha'(x)R(x))\sin\theta + \frac{\delta^2}{2}(R''(x)\alpha(x) + 2\alpha'(x)R'(x) + \alpha''(x)R(x))\sin\theta + \ldots$$

from which, ignoring terms of $0(\delta^2)$, the tangent can be found to be

$$\vec{T}_2 = T_{2x}\hat{e}_x + T_{2y}\hat{e}_y + T_{2z}\hat{e}_z \tag{5}$$

where

$$T_{2x} = 1/S_2'$$

$$T_{2y} = R'\cos\theta/S_2'$$

$$T_{2z} = (R'\alpha + \alpha'R)\sin\theta/S_2'$$

$$(S_2')^2 = \left(\frac{\partial S_2}{\partial \delta}\right)^2 \tag{6}$$

$$= 1 + (R'\cos\theta)^2 + ((R'\alpha+\alpha'R)\sin\theta)^2$$

Now, the normal can be expressed as

$$\hat{e}_n = \vec{N} = \vec{T}_1 \times \vec{T}_2 \tag{7}$$

whose components can be seen to be the following

$$e_{nx} = N_x = -(\alpha R'+\alpha' R\sin^2\theta)/D(\alpha,R,\theta)$$

$$e_{ny} = N_y = \alpha\cos\theta/D(\alpha,R,\theta)$$

$$e_{nz} = N_z = \sin\theta/D(\alpha,R,\theta)$$

$$(D(\alpha,R,\theta))^2 = \sin^2\theta + \alpha^2\cos^2\theta + (\alpha R'+\alpha' R\sin^2\theta)^2 \tag{8}$$

$\vec{p}_1$

Interplanetary plasma pressure:

$$\vec{p}_1 = -n_{ip} k T_{ip} \hat{e}_n \tag{9}$$

$\vec{p}_2$

Pressure from the component of the interplanetary magnetic field parallel to the solar wind velocity. Let α_B be defined, far from the tail, by

$$\begin{aligned} \vec{B}_{ip} \cdot \hat{e}_x &= B_{ip} \cos\alpha_B \\ \vec{B}_{ip} \cdot \hat{e}_y &= B_{ip} \sin\alpha_B \end{aligned} \tag{10}$$

Then

$$\vec{p}_2 = - \frac{(B_{ip} \cos\alpha_B)^2}{8\pi} \hat{e}_n \tag{11}$$

$\vec{p}_3$

Pressure from the component of the interplanetary magnetic field perpendicular to the solar wind velocity. Consider the problem of a cylindrical conductor of circular cross section in an externally applied magnetic field $\vec{B}_o$ which, far from the cylinder, is everywhere uniform, parallel and alligned perpendicular to the cylinder axis (in the direction, for instance of $\hat{e}_y$). This problem can be conformally transformed into the same problem with a cylinder of elliptical cross section. The problem of finding the magnetic scalar potential for the circular cylinder configuration is a standard magnetostatics exercise (see, for instance, Stratton, p. 261 ff). One such potential is

$$\Phi_M = -(\rho + \frac{\Gamma^2}{\rho}) B_o \cos\psi \frac{R\sqrt{1-\alpha^2}}{2} \tag{12}$$

where Γ is the radius of the cylinder cross section and (ρ,ψ) are standard polar coordinates.

Consider the conformal transformation illustrated in figure 3:

$$w = \frac{R\sqrt{1-\alpha^2}}{2} (\upsilon + \frac{1}{\upsilon}) \tag{13}$$

where

$$\begin{aligned} w &= y + iz \\ \upsilon &= \eta + i\zeta \end{aligned} \tag{14}$$

We then have

$$\begin{aligned} B_y(y,z) &= B_o \left[\left(1 + \frac{\Gamma^2}{\rho^2}\left(1 - \frac{2\eta^2}{\rho^2}\right)\right) \frac{\partial\eta}{\partial y} + \frac{2\Gamma^2\eta\zeta}{\rho^4} \frac{\partial\eta}{\partial z} \right] \frac{R\sqrt{1-\alpha^2}}{2} \\ B_z(y,z) &= B_o \left[\left(1 + \frac{\Gamma^2}{\rho^2}\left(1 - \frac{2\eta^2}{\rho^2}\right)\right) \frac{\partial\eta}{\partial z} - \frac{2\Gamma^2\eta\zeta}{\rho^4} \frac{\partial\eta}{\partial y} \right] \frac{R\sqrt{1-\alpha^2}}{2} \end{aligned} \tag{15}$$

where

$$\begin{aligned} \frac{\partial\eta}{\partial y} &= \frac{1}{R\sqrt{1-\alpha^2}} \left[1 + \frac{y\sqrt{1+\cos\theta_1} + z\sqrt{1-\cos\theta_1}}{\sqrt{2r_1}} \right] \\ \frac{\partial\eta}{\partial z} &= \frac{1}{R\sqrt{1-\alpha^2}} \cdot \frac{y\sqrt{1-\cos\theta_1} - z\sqrt{1+\cos\theta_1}}{\sqrt{2r_1}} \end{aligned} \tag{16}$$

where $r_1 e^{i\theta_1} = (y + iz)^2 - R^2(1-\alpha^2)$ (17)

At the surface of the cylinder, $y = R\cos\theta$ and $z = \alpha R\sin\theta$ and we have

$$B_{y,S} = B_o\left[\left(1-\eta^2/\Gamma^2\right)\frac{\partial\eta}{\partial y} + \frac{\eta\zeta}{\Gamma^2}\frac{\partial y}{\partial z}\right]R\sqrt{1-\alpha^2}$$

$$B_{z,S} = B_o\left[\left(1-\eta^2/\Gamma^2\right)\frac{\partial\eta}{\partial z} - \frac{\eta\zeta}{\Gamma^2}\frac{\partial\eta}{\partial y}\right]R\sqrt{1-\alpha^2} \qquad (18)$$

$$\frac{\partial\eta}{\partial y} = \frac{1}{R\sqrt{1-\alpha^2}}\left[1 + \frac{\alpha}{\alpha^2\cos^2\theta+\sin^2\theta}\right]$$

$$\frac{\partial\eta}{\partial z} = \frac{\sqrt{1-\alpha^2}}{R}\frac{\cos\theta\sin\theta}{\alpha^2\cos^2\theta+\sin^2\theta} \qquad (19)$$

and, of course, the hydrostatic pressure near the surface of the elliptical cylinder can be found by evaluating

$$p_3 = \frac{1}{8\pi}(B_{y,S}^2 + B_{z,S}^2) \qquad (20)$$

This is the solution for an elliptical cylinder. The more general case we are interested in here, in which the cross section changes, can be approximated by linearizing the changing dimensions of the cross section. Figure 4 shows a step-wise approximation to the surface at the intersection of the surface with the half plane $\theta = \theta_o$. The total force on the unit of surface area from x to x + δx and from θ to $\theta + \delta\theta$ is

$$\vec{F} \approx p_3(x)\left[R\delta x\hat{e}_r - ((R+\delta R)^2-R^2)\hat{e}_x\right]\delta\theta \qquad (21)$$

which is, as $\delta x \to 0$

$$\approx p_3(x)\delta n\,\hat{e}_n \qquad (22)$$

where δ_n is a differential area on the surface. So, finally

$$\vec{p}_3 = \frac{1}{8\pi}(B_{y,S}^2 + B_{z,S}^2)\hat{e}_n \qquad (23)$$

$\vec{p}_4$

Pressure from the plasma in the geomagnetic tail. To a first approximation the plasma density can be assumed to be constant everywhere in a given cross section. Thus

$$\vec{p}_4 = n_{gt} k T_{gt} \hat{e}_n \tag{24}$$

$\vec{p}_5$

Pressure from the geomagnetic field in the tail. For an elongated tail this field will have a toroidal component due to the rotation of the Earth (Dessler and Juday, 1965). Resolving the geomagnetic tail field into a toroidal component and a longitudinal component is simple in the case of a circular cross section:

$$\vec{B}_{gt} = B_{gt} \cos\varphi \hat{e}_\xi + B_{gt} \sin\varphi \hat{e}_\psi \tag{25}$$

where φ is the pitch angle of the spiral of the geomagnetic tail field:

$$\cos^2\varphi = \frac{V_p^2}{V_p^2 + \omega_E^2 R^2} \tag{26}$$

where V_p is the average velocity at which the geomagnetic plasma propagates down the tail, and ω_E is the angular velocity of the Earth. It is likely that V_p is nearly the solar wind velocity (Dessler and Juday, 1965).

Consider the problem of a toroidal magnetic field inside an elliptically cylindrical conducting shell. It can be verified that the following magnetic scalar potential satisfies Laplace's equation and the appropriate boundary conditions for the interior:

$$\Phi_M = -B_o R \sin^{-1}\left[\sqrt{(y^2+z^2+R^2(1-\alpha^2)-\sqrt{(y^2+z^2+R^2(1-\alpha^2))^2-4y^2})/2}\right] \tag{27}$$

where R and αR are, of course, the semi-major and semi-minor axes of the interior. From this potential we find

$$B^2 = \frac{B_o^2}{\sin^2\theta + \alpha^2\cos^2\theta} \tag{28}$$

and, once again using the argument illustrated in figure 4, we have

$$\vec{p}_5 = \frac{B_{gt}^2}{8\pi}\left\{\cos^2\varphi + \frac{\sin^2\varphi}{\sin^2\theta + \alpha^2\cos^2\theta}\right\}\hat{e}_n \tag{29}$$

$\vec{p}_6$

Pressure exerted by the solar wind due to its super-Alfvénic velocity. The problem of supersonic flow past a surface is well known (Cf. Landau and Lifshitz, 1959), and in this case the pressure can be shown to be

$$\vec{p}_6 \approx -\frac{\rho_{sw}V_{sw}^2}{\beta}\frac{\lambda}{(1+\lambda^2)^{1/2}}\left[1 - \frac{\beta^2+1}{2\beta}\frac{\lambda}{(1+\lambda^2)^{1/2}}\right]\hat{e}_n \tag{30}$$

where

$$\beta^2 = \frac{V_{sw}^2 - V_A^2}{V_A^2} \tag{31}$$

$$\lambda = \frac{\partial}{\partial x}(r(\theta,x)) \tag{32}$$

$$V_A = \text{Alfvén velocity} \tag{33}$$

$$= \frac{B_{ip}}{\sqrt{8\pi\rho_{sw}}}$$

Equilibrium Equations

Since, according to assumption 2, we are assuming that all cross-sections are elliptical, the configuration of the magnetopause at a given value of x can be uniquely specified by two parameters: $\alpha(x)$ and $R(x)$

(see figure 2). It is sufficient, therefore, to pick any two lines on the surface in order to obtain equilibrium equations for α and R along these lines. The natural choice for these two lines is the intersection of the surface with the half-planes $\theta = 0$ and $\theta = \pi/2$; this choice simplifies our equations considerably.

From Eq. (8)

$$(D(\alpha,R,0))^2 = \alpha^2(1+R'^2)$$

$$(D(\alpha,R,\pi/2))^2 = 1 + f^2$$

$$\hat{e}_n(\theta=0) = \frac{\hat{e}_y - R'\hat{e}_x}{(1+R'^2)^{1/2}}$$

$$\hat{e}_n(\theta=\pi/2) = \frac{\hat{e}_z - f\,\hat{e}_x}{\left[1+f^2\right]^{1/2}} \tag{34}$$

where

$$f = \alpha'R + \alpha R' \tag{35}$$

From Eq. (20)

$$\vec{p}_3(\theta=0) = \vec{0}$$

$$\vec{p}_3(\theta=\pi/2) = -\frac{(B_{ip}(1+\alpha)\sin\alpha_B)^2}{8\pi}\,\hat{e}_n(\theta=\pi/2) \tag{36}$$

From Eq. (29)

$$\vec{p}_5(\theta=0) = \frac{B_{gt}^2}{8\pi}\left(\cos^2\varphi + \frac{\sin^2\varphi}{\alpha^2}\right)\hat{e}_n(\theta=0)$$

$$\vec{p}_5(\theta=\pi/2) = \frac{B_{gt}^2}{8\pi}\,\hat{e}_n(\theta=\pi/2) \tag{37}$$

From Eqs. (32) and (30)

$$\lambda(\theta=0) = R'$$

$$\lambda(\theta=\pi/2) = f \tag{38}$$

$$\vec{p}_6(\theta=0) = -\frac{\rho_{sw}V_{sw}^2}{\beta}\frac{R'}{(1+R'^2)^{1/2}}\left[1+\frac{\beta^2+1}{2\beta}\frac{R'}{(1+R'^2)^{1/2}}\right]\hat{e}_n(\theta=0)$$

$$\vec{p}_6(\theta=\pi/2) = -\frac{\rho_{sw}V_{sw}^2}{\beta}\frac{f}{(1+f^2)^{1/2}}\left[1-\frac{\beta^2+1}{2\beta}\frac{f}{(1+f^2)^{1/2}}\right]\hat{e}_n(\theta=\pi/2) \tag{39}$$

Thus, if $\vec{p}_T$ represents the total pressure,

$$\vec{p}_T(0) = \vec{p}_T(\theta=0) = \left[-n_{ip}kT_{ip} - \frac{(B_{ip}\cos\alpha_B)^2}{8\pi} + n_{gt}kT_{gt} + \frac{B_{gt}^2}{8\pi}\left(\cos^2\varphi+\frac{\sin^2\varphi}{\alpha^2}\right)\right.$$

$$\left. - \frac{\rho_{sw}V_{sw}^2}{\beta}\frac{R'}{(1+R'^2)^{1/2}}\left(1-\frac{\beta^2+1}{2\beta}\frac{R'}{(1+R'^2)^{1/2}}\right)\right]\frac{\hat{e}_y-R'\hat{e}_x}{(1+R'^2)^{1/2}}$$

$$\vec{p}_T(\pi/2) = \vec{p}_T(\theta=\pi/2) = \left[-n_{ip}kT_{ip} - \frac{(B_{ip}\cos\alpha_B)^2}{8\pi} - \frac{(B_{ip}\sin\alpha_B)^2}{8\pi}(1+\alpha)^2\right.$$

$$\left. + n_{gt}kT_{gt} + \frac{B_{gt}^2}{8\pi} - \frac{\rho_{sw}V_{sw}^2}{\beta}\frac{f}{(1+f^2)^{1/2}}\left(1-\frac{\beta^2+1}{2\beta}\frac{f}{(1+f^2)^{1/2}}\right)\right]$$

$$\frac{\hat{e}_z-f\hat{e}_x}{(1+f^2)^{1/2}} \tag{40}$$

Now, the relation between $R(x)$, $\alpha(x)$, and $\vec{p}_T$ can be found as follows:

at $\theta = 0$:

$$\frac{dR}{dt} = \frac{\partial R}{\partial y}\frac{dy}{dt} + \frac{\partial R}{\partial x}\frac{dx}{dt} \tag{41}$$

$$\frac{d^2R}{dt^2} = \frac{dy}{dt}\left(\frac{\partial^2 R}{\partial y^2}\frac{dy}{dt} + \frac{\partial R}{\partial y}\frac{\partial}{\partial y}\left(\frac{dy}{dt}\right) + \frac{\partial^2 R}{\partial y \partial x}\frac{dx}{dt} + \frac{\partial R}{\partial x}\frac{\partial}{\partial y}\left(\frac{dx}{dt}\right)\right)$$

$$+ \frac{dx}{dt}\left(\frac{\partial^2 R}{\partial x^2}\frac{dx}{dt} + \frac{\partial R}{\partial x}\frac{\partial}{\partial x}\left(\frac{dx}{dt}\right) + \frac{\partial^2 R}{\partial x \partial y}\frac{dy}{dt} + \frac{\partial R}{\partial y}\frac{\partial}{\partial x}\left(\frac{dy}{dt}\right)\right)$$

$$+ \frac{\partial^2 R}{\partial y \partial t}\frac{dy}{dt} + \frac{\partial R}{\partial y}\frac{d^2y}{dt^2} + \frac{\partial^2 R}{\partial x \partial t}\frac{dx}{dt} + \frac{\partial R}{\partial x}\frac{d^2x}{dt^2} \tag{42}$$

Since $y = R(x)$, $dx/dt = V_x$, $dy/dt = VR'$,

$$\frac{d^2R}{dt^2} = VR'\left(\frac{\partial}{\partial y}(VR') + R'\frac{\partial}{\partial y}(V_x)\right) + V_x\left(R''V_x + R'\frac{\partial}{\partial x}V_x + \frac{\partial}{\partial x}(VR')\right)$$

$$+ \frac{p_{Ty}^{(0)}}{\rho_{mp}\tau_{mp}} + V_x\frac{\partial}{\partial t}R' + R'\frac{p_{Tx}^{(0)}}{\rho_{mp}\tau_{mp}} \tag{43}$$

which reduces to

$$R'' = \frac{-R'p_{Tx}^{(0)} + p_{Ty}^{(0)}}{\rho_{mp}\tau_{mp}(1-R'^2)(1+R'^2)^{1/2}} = \frac{p_T^{(0)}}{\rho_{mp}\tau_{mp}(1-R'^2)} \tag{44}$$

Similarly

$$\alpha'' = -2\alpha'R' - R''\alpha + \frac{-fp_{Tx}^{(\pi/2)} + p_{Tz}^{(\pi/2)}}{\rho_{mp}\tau_{mp}(1-f^2)(1+f^2)^{1/2}} \tag{45}$$

$$= -2\alpha'R' - R''\alpha + \frac{p_T^{(\pi/2)}}{\rho_{mp}\tau_{mp}(1-f^2)} \tag{46}$$

We must now specify relations expressing the variation, as a function of distance down the tail, of each of the geomagnetic and interplanetary parameters (D = 1 AU, and the positive x-axis is in the solar direction):

$$(B_{ip})_r \sim \frac{1}{(D-x)^2} \tag{47}$$

$$(B_{ip})_\theta \sim \frac{1}{D-x} \tag{48}$$

$$\rho_{sw} \sim \frac{1}{(D-x)^2} \tag{49}$$

$$V_{sw} \sim D - x \tag{50}$$

$$p_{sw} \sim \frac{1}{(D-x)^{2.3}} \tag{51}$$

$$B_{gt} \sim R_o^2/\alpha R^2 \tag{52}$$

$$\rho_{gt} \sim R_o^2/\alpha R^2 \tag{53}$$

$$p_{gt} \sim (R_o^2/\alpha R^2)^{5/3} \quad \text{(adiabatic expansion)} \tag{54}$$

Solutions and Discussion

Equations (40) and (44) to (54) constitute a well defined set of two coupled, second order, ordinary differential equations for two dependent variables R(x) and $\alpha(x)$ and one independent variable x. Due to the complex nature of these equations, they are not amenable to analytic solution. They can, however, be handled quite readily by any of several numerical techniques. In order to integrate these equations numerically, the various parameters in the problem were assigned the following values (at $x_{SM} \approx -20\ R_E$):

$B_{ip} = 5.0\gamma$

$n_{ip} = 7.0\ cm^{-3}$

$T_{ip} = 2.0 \times 10^5\ ^oK$

$V_{sw} = 400$ km/sec

$|\cos^{-1}|B_{ip}\cdot B_{gt}||= 45^{o}$

$B_{gt} = 10.0\ \gamma$

$n_{gt} = 0.10\ cm^{-3}$

$T_{gt} = 1.0x10^{6}\ ^{o}K$

B_{gt} pitch angle = $3.2x10^{-3}$ radians

$r_{mp} = 100$ km

$n_{mp} = 100\ cm^{-3}$

Using a four-point predictor-corrector method (Milne) with Runge-Kutta starter, the following initial conditions:

$R_o = 25.0\ R_E$

$R'_o = 0.0$

$\alpha_o = 1.0$

$\alpha'_o = 0.0\ R_E^{-1}$

and a step size of 0.40 R_E, the differential equations were integrated from $x_{SM} = -20\ R_E$ to $x_{SM} = -1520\ R_E$. The results of this integration are shown in figure 5, where the following quantities are plotted as a function of distance along the geomagnetic tail axis ($-x_{SM}$ axis) from the point $x_{SM} = -20\ R_E$: the semi-major and semi-minor axes of the elliptical cross section, and the eccentricity, e, of the ellipse. The eccentricity is related to $\alpha(x)$ by

$$e = \sqrt{1-\alpha^2} \qquad \alpha \leq 1$$
$$= \frac{\sqrt{\alpha^2-1}}{\alpha} \qquad \alpha \geq 1 \tag{55}$$

The variations in the cross sectional dimensions of the tail indicated for distances $\lesssim 200\ R_E$ are not real and merely indicate an adjustment of the solution to a non-consistent set of initial conditions.

In order to determine the sensitivity of this numerical solution to the accuracy of the values chosen for the geomagnetic and interplanetary parameters, a series of solutions of this type were generated wherein each parameter was varied in turn by ± 20% and ± 40% (except α_o, which was varied from 0.6 to 1.0 in steps of 0.1). These solutions are displayed in Figures 6 to 19, where each figure illustrates the effect of varying a single parameter. Several observations can be made (by "width" we will mean "semi-major axis" and by "thickness" we will mean "semi-minor axis"):

Specific

1. The strength of the interplanetary magnetic field seems to have almost no effect on the width of the tail, and the thickness only decreased by ~ 9% for a 40% increase in the field strength.

2. Variations in the temperature and density of the interplanetary plasma showed just what one would expect: larger or smaller cross-sectional dimensions, but no significant change in eccentricity.

3. Variations in the solar wind velocity show no major effects. The instability in the solution for the smallest velocity (240 km/sec) is more characteristic of the numerical method than of real instabilities. Recalculation of this solution with a smaller step size indicated that the "instability" was indeed method-dependent.

4. The effect of changing the angle between the interplanetary magnetic field and the geomagnetic tail axis were somewhat surprising. Especially at the larger angles, there was hardly any effect on the ultimate thickness of the tail. Variations in the eccentricity merely reflect significant variations in the width.

5. Since the geomagnetic field strength plays the dominant role (at least in terms of internal forces) in determining the size of the tail, while the toroidal component resists the anisotropic pressure of the interplanetary magnetic field, the results shown in figure 10 are what one would expect. A 40% increase in the strength of the geomagnetic tail field results in a $\sim$ 40% increase in the cross-sectional area of the tail, and a smaller eccentricity.

6. Figures 11 and 12 are consistent with the idea that the geomagnetic tail plasma plays an insignificant role, and that any variations, therefore, have very little effect. This makes some of the somewhat cavalier assumptions concerning the spatial distribution of this plasma less significant.

7. In light of the Michel and Dessler argument, the effects of changing the pitch angle of the geomagnetic tail field are surprising. Michel and Dessler (1970) propose that the toroidal component of the geomagnetic tail field gives rise to one of the dominant forces opposing the anisotropic pressure of the interplanetary magnetic field. Variations in this component of $\pm$ 40% have, however, no discernible effect on the cross sectional shape of the distant geomagnetic tail, at least in the context of the present study.

8. Variations in the characteristics of the magnetopause indicate no effect on the solution, with one exception: if either the number density or the thickness become too small, instabilities appear in the solution. As with V_{sw}, these instabilities do not represent real, physical instabilities, but are, rather, a function of the characteristics of the numerical integration technique and precision of the computer used. Again, as in the case of the instabilities encountered with V_{sw}, when

steps were taken toward more precision in the solution (smaller step size and/or double precision calculations) the instabilities were no longer apparent.

9. Changes in R_o did little but change the overall size of the cross section. Since this in turn changed the amount by which the interplanetary field was distorted, the eccentricity was affected.

10. Changing α_o seems to have little effect on the ultimate dimensions of the tail cross section with the single exception that if α_o is much too low (or high, presumably) oscillations are set up in the solutions which do not damp out.

General

11. It is reassuring that many of the parameters which are most critical in the solution (e.g., B_{ip}, B_{gt}, n_{ip}) are also among the best known, while some of the values least well known (e.g., n_{gt}, n_{mp}) have very small influence over the final configuration.

12. Figures 16 and 17 (variations of R_o and α_o) indicate that $R_o \approx 27\ R_E$ and $\alpha_o \approx 0.9$ may be better initial values, but these figures also indicate that the ultimate shape of the tail cross section is relatively insensitive to variations in R_o and α_o like these ($\sim 8\%$ in R_o and $\sim 10\%$ in α_o).

With the confidence, then, that the solutions are at least behaving reasonably and that the parameters suspected of being the least accurate are also the least significant, this solution can be extended out to $\sim 10^4\ R_E$. The results are shown in figure 20 for the parameter values discussed above. The two major observations to be made from this solution are:

1. Beyond $\sim 3 \times 10^3\ R_E$ the tail becomes wider, but no thinner (one does indeed expect an increasing cross sectional

area, of course, since the interplanetary pressures are decreasing with increasing distance from the sun).

2. This solution does not support the assumption of Michel and Dessler (1970) that at $\sim 10^4$ R_E the tail will be $\sim 10^3$ R_E wide and ~ 10 R_E thick.

Considering the second of these observations first, if the indications of this solution are valid, they might have serious consequences for the particle access model of Michel and Dessler (1970). The method which they proposed by which electrons and low energy protons were to gain rapid access to open geomagnetic field lines relied heavily on the geomagnetic tail becoming filamentary. The process by which the tail was to become filamentary relied, in turn, on the tail becoming very wide and very thin ($\sim 10^3$ R_E x ~ 10 R_E). If the tail does not become so drastically thin, then a mechanism by which the tail can become filamentary is not at all obvious. If the tail does not become filamentary, then the method which they have proposed for the rapid access of low rigidity particles is no longer applicable.

In addition, considering the first observation, it does not appear from figure 20 that the tail cross section would ever approach such extreme eccentricity: the semi-minor axis even seems to have a minimum at $\sim 5 \times 10^3$ R_E and at $\sim 10^4$ R_E is increasing slightly.

This study has, of course, been predicated on some rather severe assumptions, and one could undoubtedly have more confidence in the accuracy of a solution in which these assumptions were relaxed. Nevertheless, within the limitations of these assumptions the solutions obtained are consistent and reasonable, and the implications of these solutions are straightforward.

Figure Captions

1. Representation of the shape of the distant geomagnetic tail, defining the coordinate system used in this study and showing the curves used in defining $\hat{e}_n$.

2. Cross sectional view of distant tail showing the inter-relationships among the variables discussed in the text.

3. Conformal transformation used to treat anisotropic pressures.

4. Illustration of the approximation involving linearization of the variations in the cross section as a function of distance down the tail.

5. Solution to equilibrium equations for typical values of geomagnetic and interplanetary parameters. "Distance" is measured along the $-x_{SM}$ axis from $x_{SM} = -20\ R_E$.

Figures 6 through 18

Investigation of the sensitivity of the solution to the equilibrium equations for the surface of the geomagnetic tail shown in figure 5 to the values of the geomagnetic and interplanetary parameters. Each of the following parameters is varied in turn, usually by ± 10% and ± 20%:

Figure	Parameter Varied	Values	Parameter Description
6	B_{ip}	3.0(1.0)5.0 γ *	Interplanetary magnetic field strength.
7	n_{ip}	4.2(1.4)9.8 cm^{-3}	Number density of interplanetary plasma.
8	T_{ip}	1.2(0.4)2.8 $^{o}Kx10^{5}$	Temperature of interplanetary plasma.
9	V_{sw}	240(80)560 km/sec	Solar wind velocity.
10	$\lvert\cos^{-1}\lvert\vec{B}_{gt}\cdot\vec{B}_{ip}\rvert\rvert$	27°(9°)63°	Acute angle between interplanetary magnetic field and geomagnetic field.
11	B_{gt}	6(2)14 γ	Geomagnetic field strength in tail.
12	n_{gt}	0.06(0.02)0.14 cm^{-3}	Number density of plasma in tail.
13	T_{gt}	0.6(0.2)1.4 $^{o}Kx10^{6}$	Temperature of plasma in tail.
14	B_{gt} pitch a.	1.9(0.6)4.5 radians x 10^{-3}	Pitch angle of geomagnetic tail field.
15	mp	60(20)140 km	Thickness of magnetopause.
16	n_{mp}	60(20)140 cm^{-3}	Number density of magnetopause plasma.
17	R_o	15(5)35 R_E	Semi-major axis of cross section of geomagnetic tail at x_{SM} = -20 R_E.
18	α_o	0.6(0.1)1.0	Ratio of minor axis to major axis of geomagnetic tail cross section at x_{SM} = -20 R_E.

*This notation indicates that the parameter was varied from 3 to 5 in steps of 1.

Figure 19 Extension of the solution shown in figure 5 to $\sim 10^4$ R_E. This is the distance by which Michel and Dessler (1970) predict a semi-major axis of $\sim 10^3$ R_E and an eccentricity of $\sim (1 - 10^{-5})$ (or $\alpha \approx 5 \times 10^{-3}$). This study would indicate typical values at $\sim 10^4$ R_E of 55 R_E for the semi-major axis and of ~ 0.9 (or $\alpha \approx 0.44$) for the eccentricity.

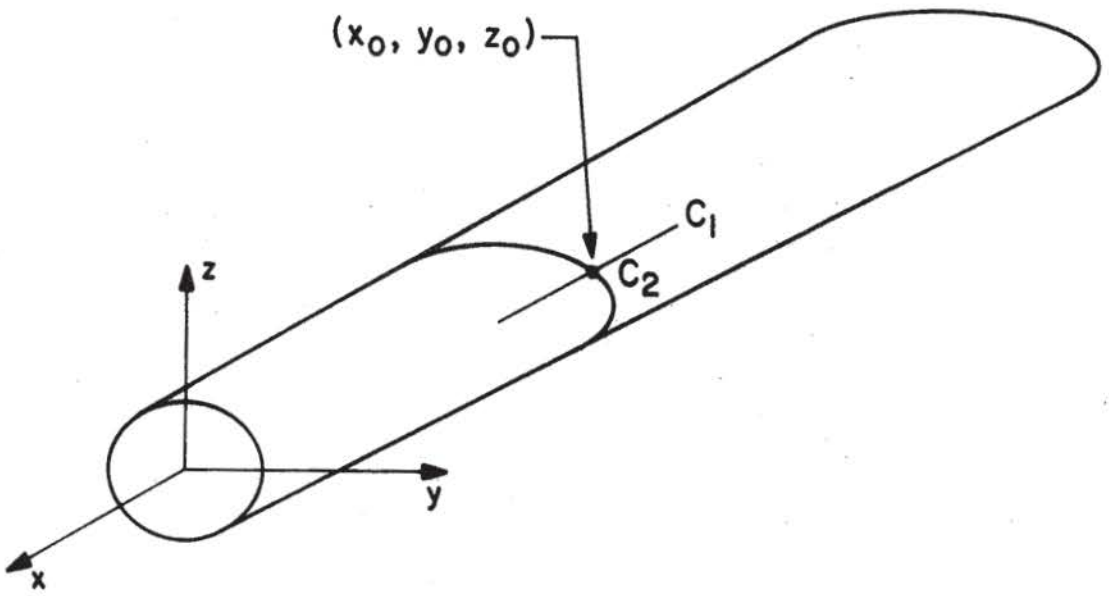

Figure 1

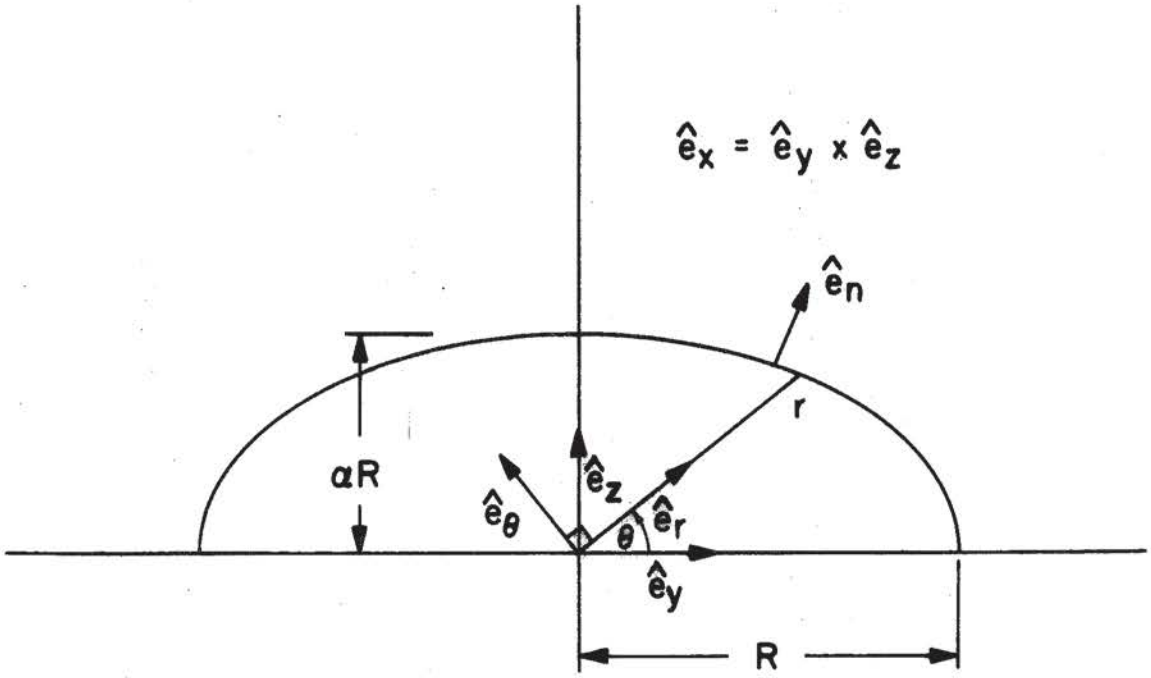
$\hat{e}_x = \hat{e}_y \times \hat{e}_z$
$\hat{e}_n$
r
αR
$\hat{e}_z$
$\hat{e}_\theta$
$\hat{e}_r$
θ
$\hat{e}_y$
R

Figure 2

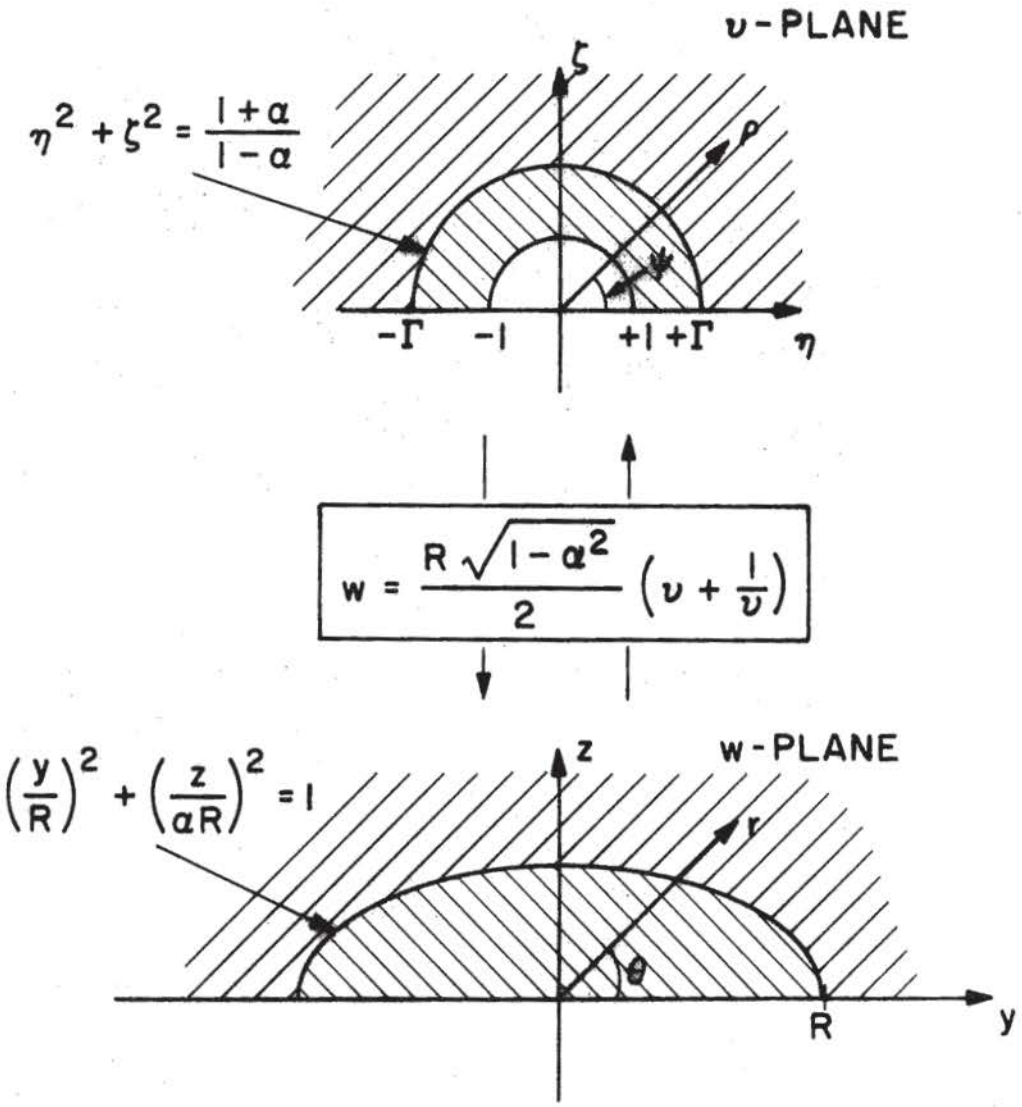
υ-PLANE
$\eta^2 + \zeta^2 = \frac{1+\alpha}{1-\alpha}$
ζ
ρ
φ
-Γ
-1
+1
+Γ
η
$w = \frac{R\sqrt{1-\alpha^2}}{2}\left(\upsilon + \frac{1}{\upsilon}\right)$
w-PLANE
$\left(\frac{y}{R}\right)^2 + \left(\frac{z}{\alpha R}\right)^2 = 1$
z
r
θ
R
y

Figure 3

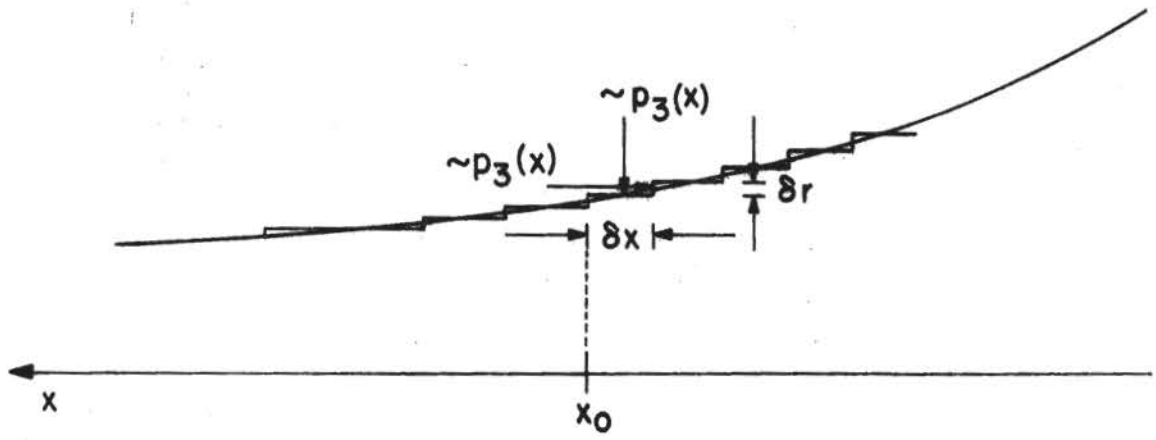

Figure 4

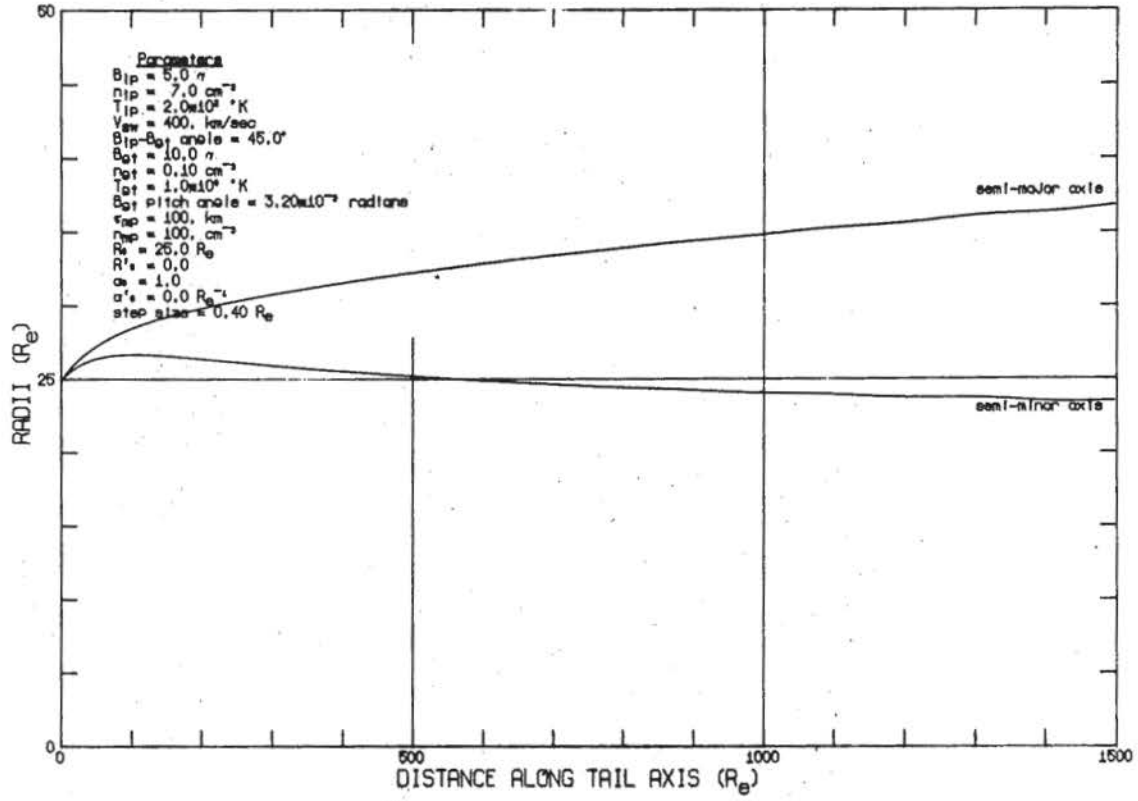
Parameters
B_{lp} = 5.0 γ
n_{lp} = 7.0 cm^{-3}
T_{lp} = 2.0x10^6 °K
V_{sw} = 400. km/sec
B_{lp}-B_{gt} angle = 45.0°
B_{gt} = 10.0 γ
n_{gt} = 0.10 cm^{-3}
T_{gt} = 1.0x10^8 °K
B_{gt} pitch angle = 3.20x10^{-3} radians
r_{mp} = 100. km
n_{mp} = 100. cm^{-3}
R_e = 25.0 R_e
R'$_s$ = 0.0
α_s = 1.0
α'_s = 0.0 R_e^{-1}
step size = 0.40 R_e
semi-major axis
semi-minor axis
RADII (R_e)
50
25
0
0
500
1000
1500
DISTANCE ALONG TAIL AXIS (R_e)

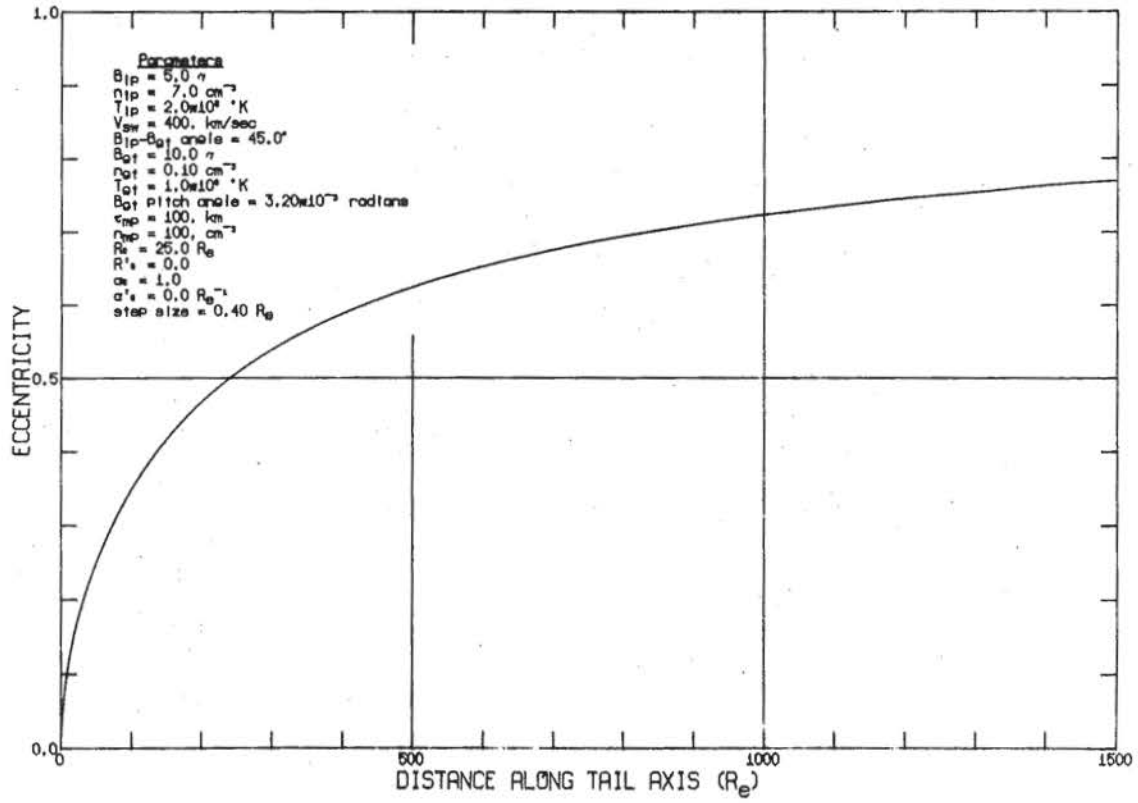
Parameters
B_{lp} = 5.0 γ
n_{lp} = 7.0 cm^{-3}
T_{lp} = 2.0x10^6 °K
V_{sw} = 400. km/sec
B_{lp}-B_{gt} angle = 45.0°
B_{gt} = 10.0 γ
n_{gt} = 0.10 cm^{-3}
T_{gt} = 1.0x10^8 °K
B_{gt} pitch angle = 3.20x10^{-3} radians
r_{mp} = 100. km
n_{mp} = 100. cm^{-3}
R_e = 25.0 R_e
R'$_s$ = 0.0
α_s = 1.0
α'_s = 0.0 R_e^{-1}
step size = 0.40 R_e
ECCENTRICITY
1.0
0.5
0.0
0
500
1000
1500
DISTANCE ALONG TAIL AXIS (R_e)

Figure 5

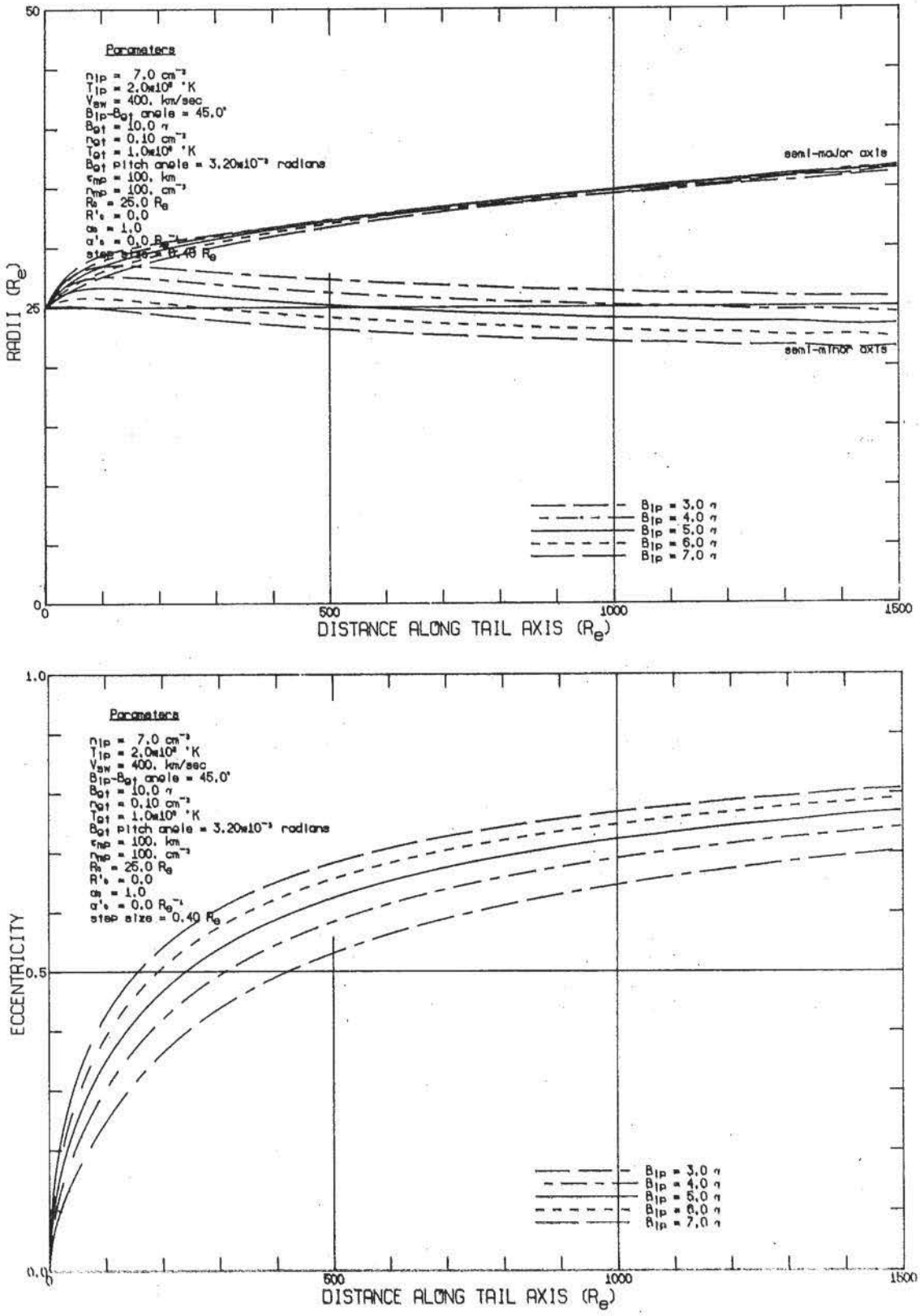
Parameters
n_{lp} = 7.0 cm^{-3}
T_{lp} = 2.0x10^{8} °K
V_{sw} = 400. km/sec
B_{lp}-B_{gt} angle = 45.0°
B_{gt} = 10.0 γ
n_{gt} = 0.10 cm^{-3}
T_{gt} = 1.0x10^{8} °K
B_{gt} pitch angle = 3.20x10^{-3} radians
r_{mp} = 100. km
n_{mp} = 100. cm^{-3}
R_s = 26.0 R_e
R'$_s$ = 0.0
α_s = 1.0
α'_s = 0.0 R_e^{-1}
step size = 0.40 R_e
semi-major axis
semi-minor axis
B_{lp} = 3.0 γ
B_{lp} = 4.0 γ
B_{lp} = 5.0 γ
B_{lp} = 6.0 γ
B_{lp} = 7.0 γ
RADII (R_e)
50
25
0
0
500
1000
1500
DISTANCE ALONG TAIL AXIS (R_e)
Parameters
n_{lp} = 7.0 cm^{-3}
T_{lp} = 2.0x10^{8} °K
V_{sw} = 400. km/sec
B_{lp}-B_{gt} angle = 45.0°
B_{gt} = 10.0 γ
n_{gt} = 0.10 cm^{-3}
T_{gt} = 1.0x10^{8} °K
B_{gt} pitch angle = 3.20x10^{-3} radians
r_{mp} = 100. km
n_{mp} = 100. cm^{-3}
R_s = 26.0 R_e
R'$_s$ = 0.0
α_s = 1.0
α'_s = 0.0 R_e^{-1}
step size = 0.40 R_e
B_{lp} = 3.0 γ
B_{lp} = 4.0 γ
B_{lp} = 5.0 γ
B_{lp} = 6.0 γ
B_{lp} = 7.0 γ
ECCENTRICITY
1.0
0.5
0.0
0
500
1000
1500
DISTANCE ALONG TAIL AXIS (R_e)

Figure 6

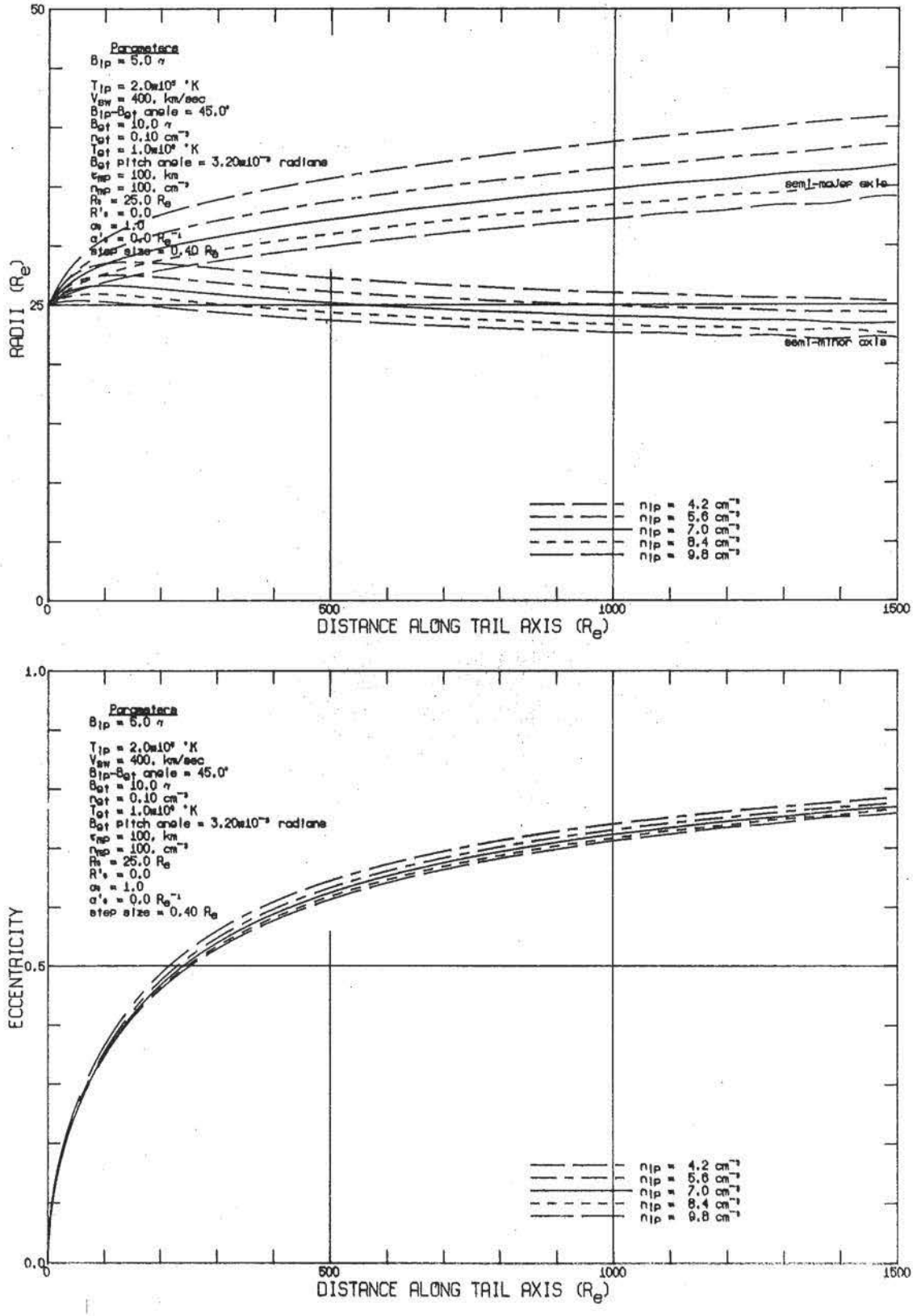
Parameters
B_{lp} = 5.0 γ
T_{lp} = 2.0×10⁸ °K
V_{sw} = 400. km/sec
B_{lp}-B_{at} angle = 45.0°
B_{at} = 10.0 γ
n_{at} = 0.10 cm⁻³
T_{at} = 1.0×10⁸ °K
B_{at} pitch angle = 3.20×10⁻³ radians
r_{mp} = 100. km
n_{mp} = 100. cm⁻³
R_s = 25.0 R_e
R'$_s$ = 0.0
α_s = 1.0
α'_s = 0.0 R_e^{-1}
step size = 0.40 R_e
semi-major axis
semi-minor axis
n_{lp} = 4.2 cm⁻³
n_{lp} = 5.6 cm⁻³
n_{lp} = 7.0 cm⁻³
n_{lp} = 8.4 cm⁻³
n_{lp} = 9.8 cm⁻³
RADII (R_e)
50
25
0
0
500
1000
1500
DISTANCE ALONG TAIL AXIS (R_e)
Parameters
B_{lp} = 5.0 γ
T_{lp} = 2.0×10⁸ °K
V_{sw} = 400. km/sec
B_{lp}-B_{at} angle = 45.0°
B_{at} = 10.0 γ
n_{at} = 0.10 cm⁻³
T_{at} = 1.0×10⁸ °K
B_{at} pitch angle = 3.20×10⁻³ radians
r_{mp} = 100. km
n_{mp} = 100. cm⁻³
R_s = 25.0 R_e
R'$_s$ = 0.0
α_s = 1.0
α'_s = 0.0 R_e^{-1}
step size = 0.40 R_e
n_{lp} = 4.2 cm⁻³
n_{lp} = 5.6 cm⁻³
n_{lp} = 7.0 cm⁻³
n_{lp} = 8.4 cm⁻³
n_{lp} = 9.8 cm⁻³
ECCENTRICITY
1.0
0.5
0.0
0
500
1000
1500
DISTANCE ALONG TAIL AXIS (R_e)

Figure 7

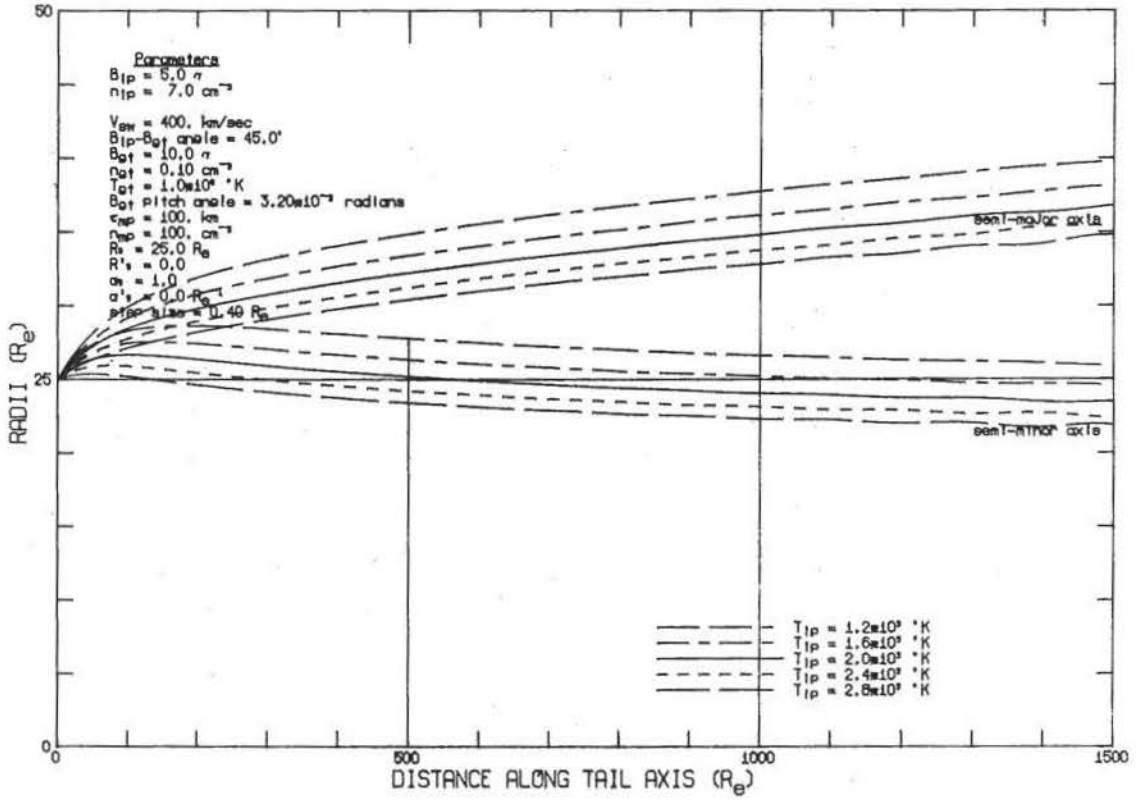
Parameters
B_{ip} = 5.0 γ
n_{ip} = 7.0 cm^{-3}
V_{sw} = 400. km/sec
B_{ip}-B_{at} angle = 45.0°
B_{at} = 10.0 γ
n_{at} = 0.10 cm^{-3}
T_{at} = 1.0×10^{8} °K
B_{at} pitch angle = 3.20×10^{-1} radians
r_{mp} = 100. km
n_{mp} = 100. cm^{-3}
R_s = 25.0 R_e
R'$_s$ = 0.0
α_s = 1.0
α'_s = 0.0 R_e^{-1}
step size = 0.40 R_e
semi-major axis
semi-minor axis
T_{ip} = 1.2×10^{8} °K
T_{ip} = 1.6×10^{8} °K
T_{ip} = 2.0×10^{8} °K
T_{ip} = 2.4×10^{8} °K
T_{ip} = 2.8×10^{8} °K
RADII (R_e)
50
25
0
0
500
1000
1500
DISTANCE ALONG TAIL AXIS (R_e)

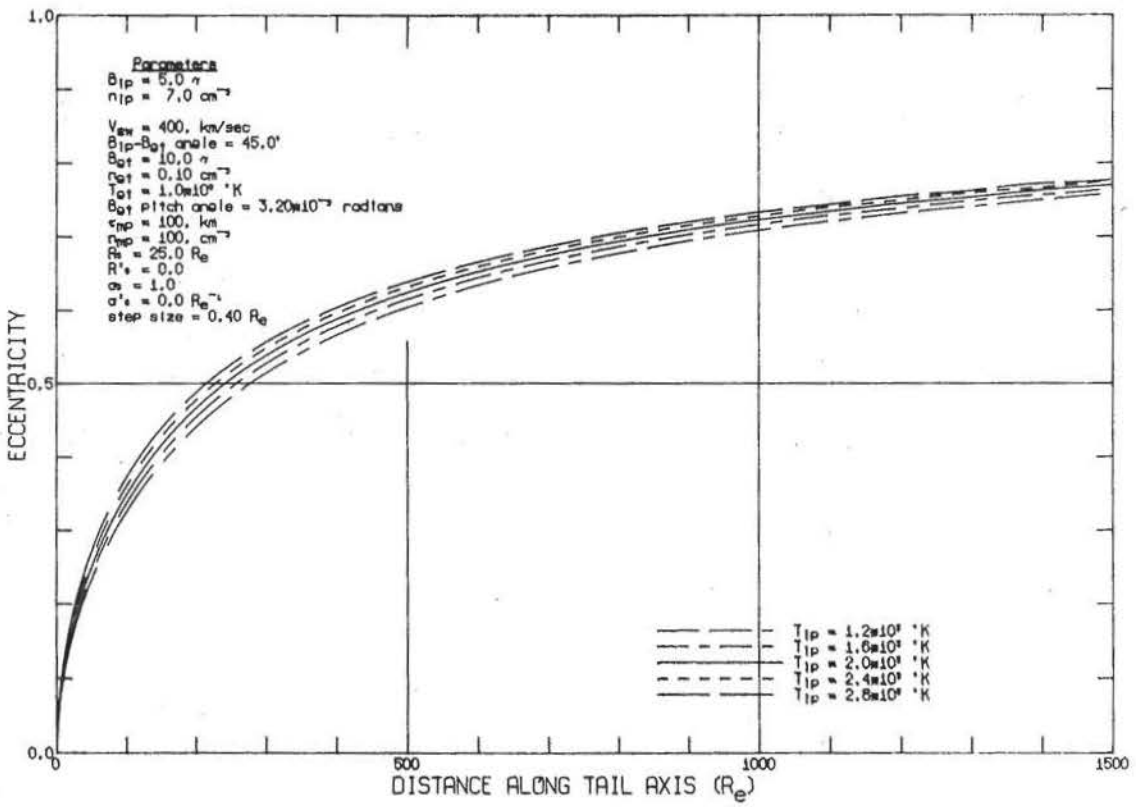
Parameters
B_{ip} = 5.0 γ
n_{ip} = 7.0 cm^{-3}
V_{sw} = 400. km/sec
B_{ip}-B_{at} angle = 45.0°
B_{at} = 10.0 γ
n_{at} = 0.10 cm^{-3}
T_{at} = 1.0×10^{8} °K
B_{at} pitch angle = 3.20×10^{-1} radians
r_{mp} = 100. km
n_{mp} = 100. cm^{-3}
R_s = 25.0 R_e
R'$_s$ = 0.0
α_s = 1.0
α'_s = 0.0 R_e^{-1}
step size = 0.40 R_e
T_{ip} = 1.2×10^{8} °K
T_{ip} = 1.6×10^{8} °K
T_{ip} = 2.0×10^{8} °K
T_{ip} = 2.4×10^{8} °K
T_{ip} = 2.8×10^{8} °K
ECCENTRICITY
1.0
0.5
0.0
0
500
1000
1500
DISTANCE ALONG TAIL AXIS (R_e)

Figure 8

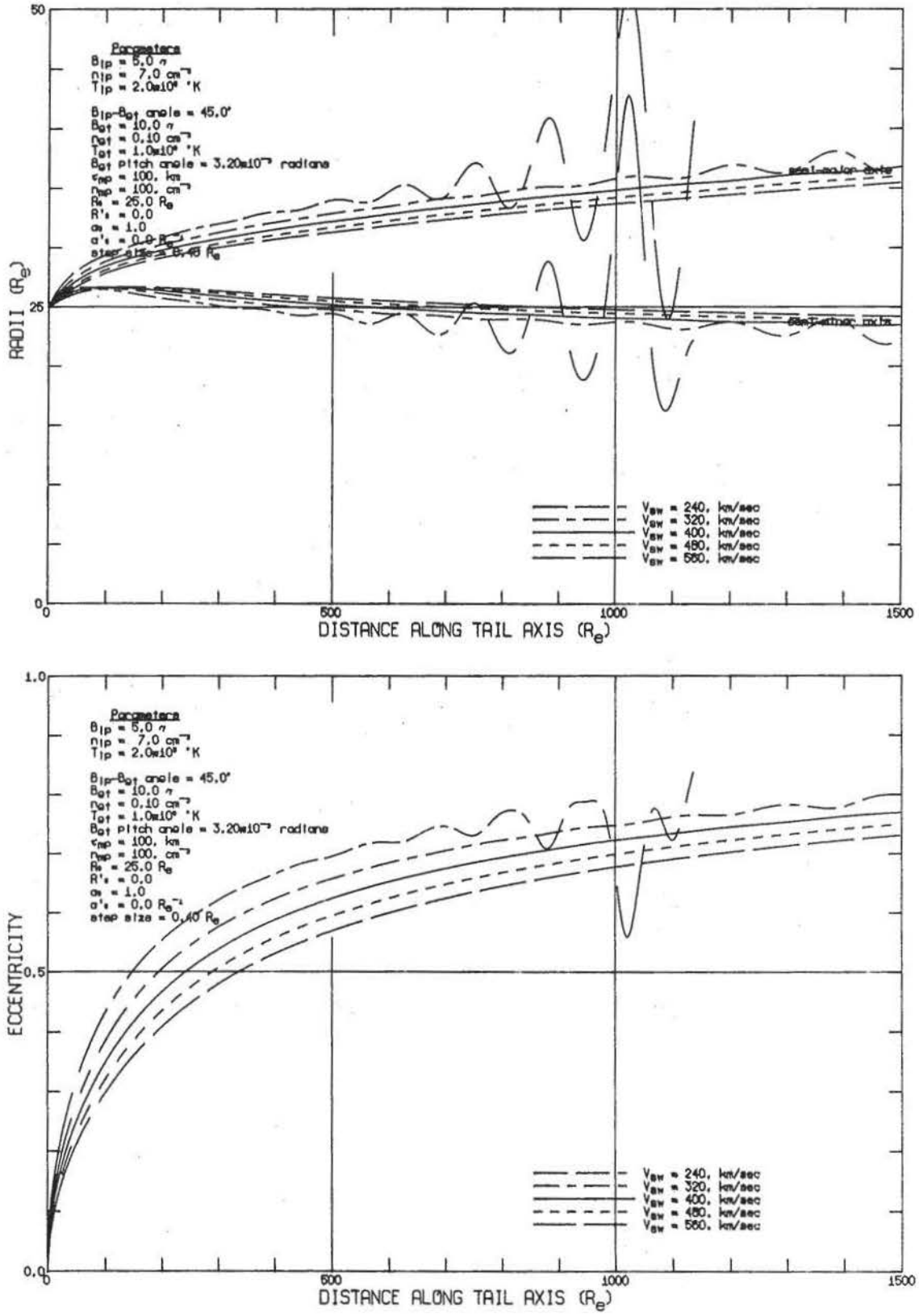
Parameters
B_{ip} = 5.0 γ
n_{ip} = 7.0 cm^{-3}
T_{ip} = 2.0x10^6 °K
B_{ip}-B_{at} angle = 45.0°
B_{at} = 10.0 γ
n_{at} = 0.10 cm^{-3}
T_{at} = 1.0x10^6 °K
B_{at} pitch angle = 3.20x10^{-3} radians
ϵ_{mp} = 100. km
n_{mp} = 100. cm^{-3}
R_s = 25.0 R_e
R'$_s$ = 0.0
α_s = 1.0
α'_s = 0.0 R_e^{-1}
step size = 0.40 R_e
semi-major axis
semi-minor axis
V_{sw} = 240. km/sec
V_{sw} = 320. km/sec
V_{sw} = 400. km/sec
V_{sw} = 480. km/sec
V_{sw} = 560. km/sec
RADII (R_e)
DISTANCE ALONG TAIL AXIS (R_e)
ECCENTRICITY
DISTANCE ALONG TAIL AXIS (R_e)

Figure 9

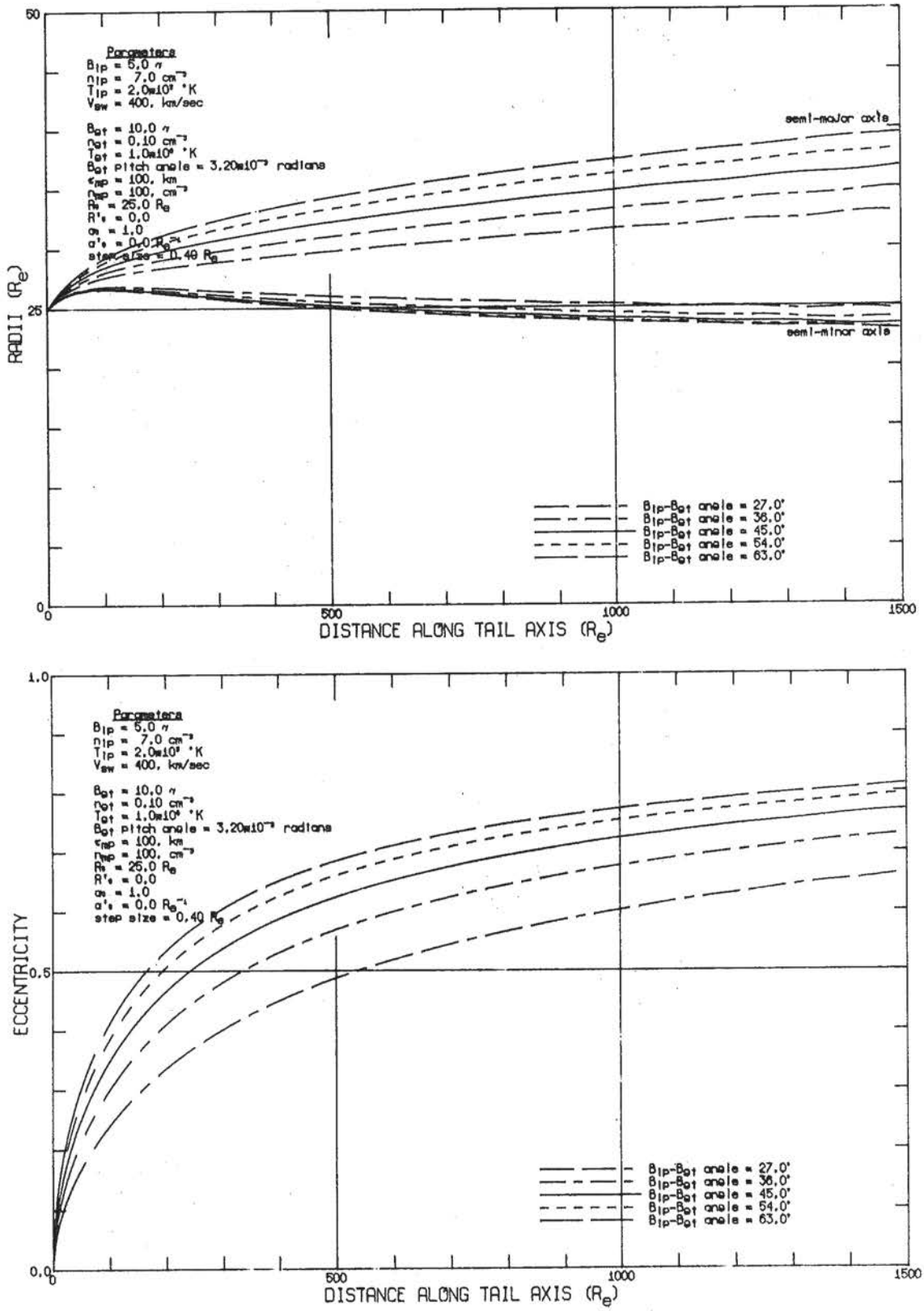
Parameters
B_{lp} = 5.0 γ
n_{lp} = 7.0 cm^{-3}
T_{lp} = 2.0x10^{6} °K
V_{sw} = 400. km/sec
B_{ot} = 10.0 γ
n_{ot} = 0.10 cm^{-3}
T_{ot} = 1.0x10^{8} °K
B_{ot} pitch angle = 3.20x10^{-3} radians
ϵ_{mp} = 100. km
n_{mp} = 100. cm^{-3}
R_a = 25.0 R_e
R'$_a$ = 0.0
α_0 = 1.0
α'_0 = 0.0 R_e^{-1}
step size = 0.40 R_e
semi-major axis
semi-minor axis
B_{lp}-B_{ot} angle = 27.0°
B_{lp}-B_{ot} angle = 36.0°
B_{lp}-B_{ot} angle = 45.0°
B_{lp}-B_{ot} angle = 54.0°
B_{lp}-B_{ot} angle = 63.0°
RADII (R_e)
50
25
0
0
500
1000
1500
DISTANCE ALONG TAIL AXIS (R_e)
Parameters
B_{lp} = 5.0 γ
n_{lp} = 7.0 cm^{-3}
T_{lp} = 2.0x10^{6} °K
V_{sw} = 400. km/sec
B_{ot} = 10.0 γ
n_{ot} = 0.10 cm^{-3}
T_{ot} = 1.0x10^{8} °K
B_{ot} pitch angle = 3.20x10^{-3} radians
ϵ_{mp} = 100. km
n_{mp} = 100. cm^{-3}
R_a = 25.0 R_e
R'$_a$ = 0.0
α_0 = 1.0
α'_0 = 0.0 R_e^{-1}
step size = 0.40 R_e
B_{lp}-B_{ot} angle = 27.0°
B_{lp}-B_{ot} angle = 36.0°
B_{lp}-B_{ot} angle = 45.0°
B_{lp}-B_{ot} angle = 54.0°
B_{lp}-B_{ot} angle = 63.0°
ECCENTRICITY
1.0
0.5
0.0
0
500
1000
1500
DISTANCE ALONG TAIL AXIS (R_e)

Figure 10

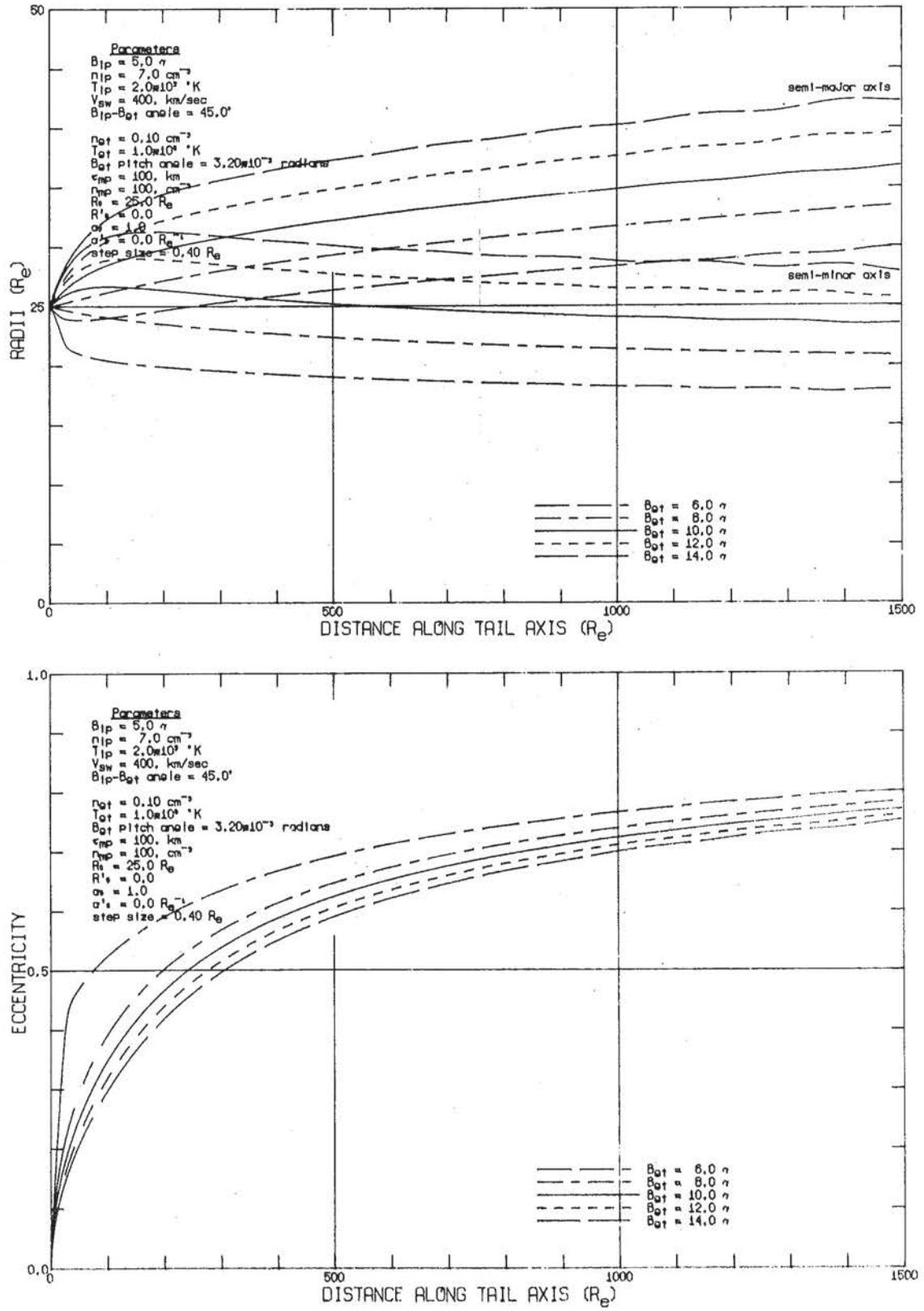
Parameters
B_{lp} = 5.0 γ
n_{lp} = 7.0 cm^{-3}
T_{lp} = 2.0×10^{7} °K
V_{sw} = 400. km/sec
B_{lp}-B_{ot} angle = 45.0°
n_{ot} = 0.10 cm^{-3}
T_{ot} = 1.0×10^{8} °K
B_{ot} pitch angle = 3.20×10^{-3} radians
ϵ_{mp} = 100. km
n_{mp} = 100. cm^{-3}
R_s = 25.0 R_e
R'$_s$ = 0.0
α_s = 1.0
α'_s = 0.0 R_e^{-1}
step size = 0.40 R_e
semi-major axis
semi-minor axis
B_{ot} = 6.0 γ
B_{ot} = 8.0 γ
B_{ot} = 10.0 γ
B_{ot} = 12.0 γ
B_{ot} = 14.0 γ
RADII (R_e)
DISTANCE ALONG TAIL AXIS (R_e)
ECCENTRICITY
0
25
50
500
1000
1500
0.0
0.5
1.0

Figure 11

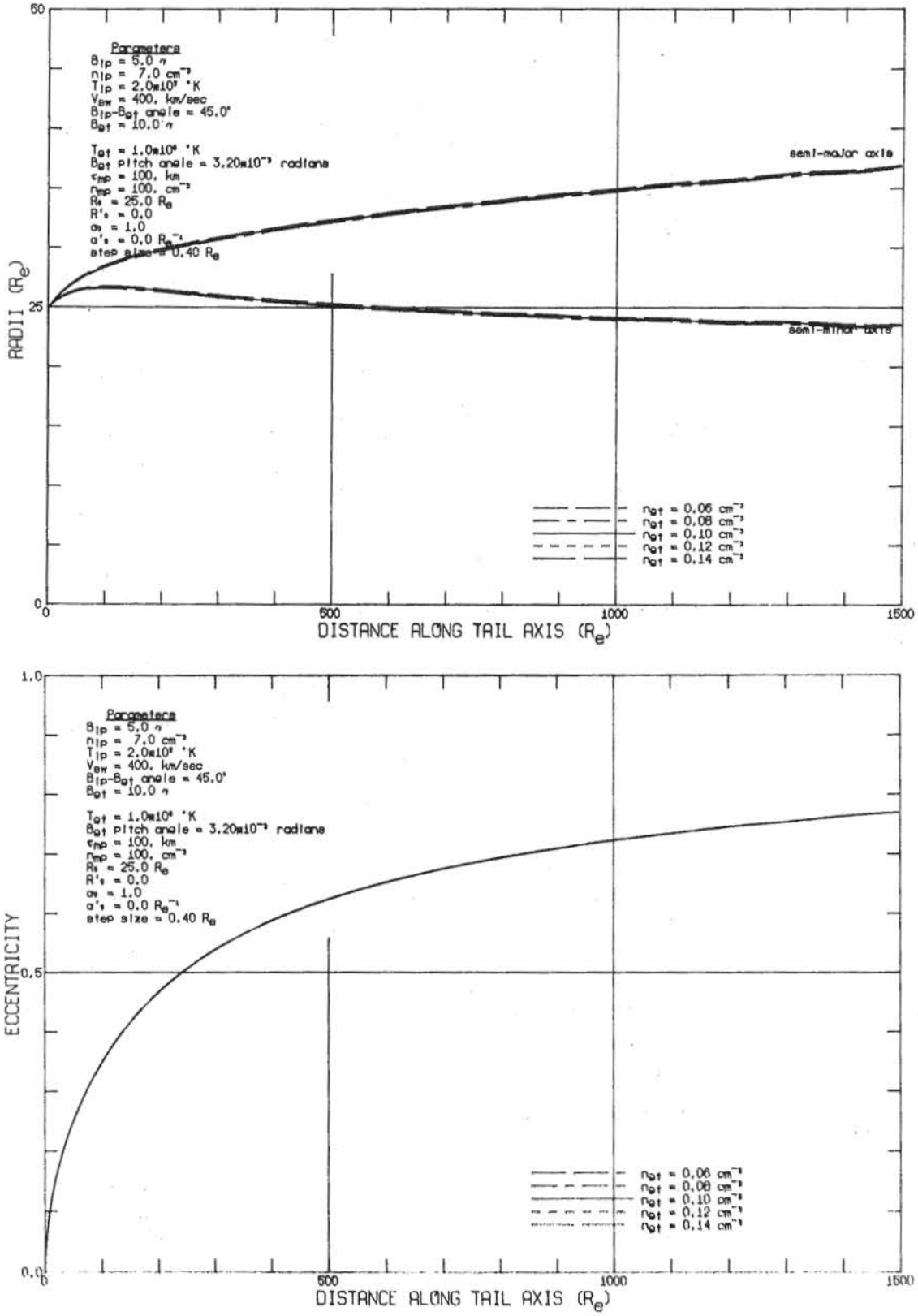
Parameters
B_{ip} = 5.0 γ
n_{ip} = 7.0 cm^{-3}
T_{ip} = 2.0x10^{8} °K
V_{sw} = 400. km/sec
B_{ip}-B_{at} angle = 45.0°
B_{at} = 10.0 γ
T_{at} = 1.0x10^{8} °K
B_{at} pitch angle = 3.20x10^{-3} radians
r_{mp} = 100. km
n_{mp} = 100. cm^{-3}
R_s = 25.0 R_e
R'$_s$ = 0.0
α_s = 1.0
α'_s = 0.0 R_e^{-1}
step size = 0.40 R_e
semi-major axis
semi-minor axis
n_{at} = 0.06 cm^{-3}
n_{at} = 0.08 cm^{-3}
n_{at} = 0.10 cm^{-3}
n_{at} = 0.12 cm^{-3}
n_{at} = 0.14 cm^{-3}
RADII (R_e)
50
25
0
0
500
1000
1500
DISTANCE ALONG TAIL AXIS (R_e)
Parameters
B_{ip} = 5.0 γ
n_{ip} = 7.0 cm^{-3}
T_{ip} = 2.0x10^{8} °K
V_{sw} = 400. km/sec
B_{ip}-B_{at} angle = 45.0°
B_{at} = 10.0 γ
T_{at} = 1.0x10^{8} °K
B_{at} pitch angle = 3.20x10^{-3} radians
r_{mp} = 100. km
n_{mp} = 100. cm^{-3}
R_s = 25.0 R_e
R'$_s$ = 0.0
α_s = 1.0
α'_s = 0.0 R_e^{-1}
step size = 0.40 R_e
n_{at} = 0.06 cm^{-3}
n_{at} = 0.08 cm^{-3}
n_{at} = 0.10 cm^{-3}
n_{at} = 0.12 cm^{-3}
n_{at} = 0.14 cm^{-3}
ECCENTRICITY
1.0
0.5
0.0
0
500
1000
1500
DISTANCE ALONG TAIL AXIS (R_e)

Figure 12

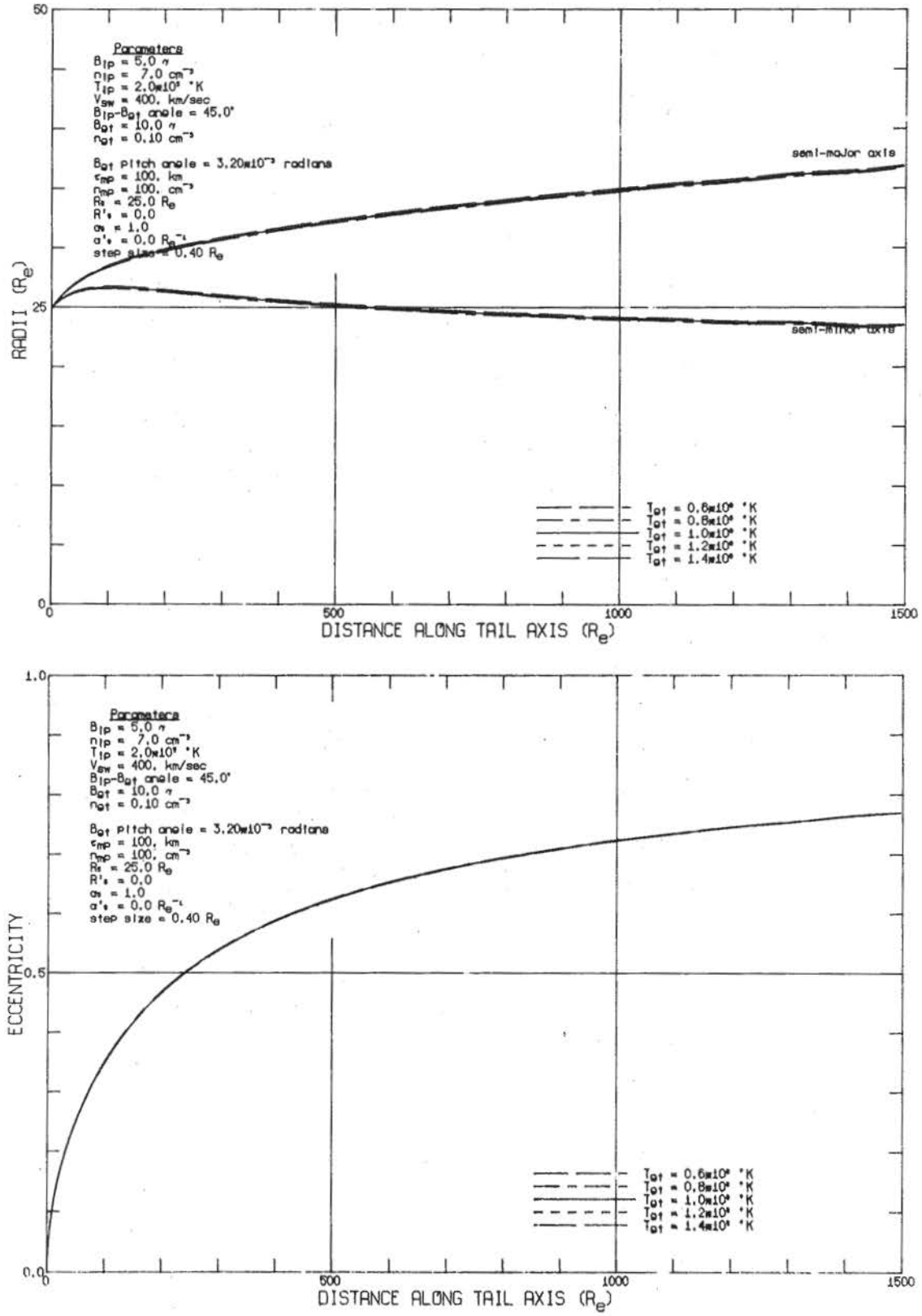
Parameters
B_{lp} = 5.0 γ
n_{lp} = 7.0 cm^{-3}
T_{lp} = 2.0×10^{8} °K
V_{sw} = 400. km/sec
B_{lp}-B_{ot} angle = 45.0°
B_{ot} = 10.0 γ
n_{ot} = 0.10 cm^{-3}
B_{ot} pitch angle = 3.20×10^{-3} radians
r_{mp} = 100. km
n_{mp} = 100. cm^{-3}
R_s = 25.0 R_e
R'_s = 0.0
α_s = 1.0
α'_s = 0.0 R_e^{-1}
step size = 0.40 R_e
semi-major axis
semi-minor axis
T_{ot} = 0.6×10^{8} °K
T_{ot} = 0.8×10^{8} °K
T_{ot} = 1.0×10^{8} °K
T_{ot} = 1.2×10^{8} °K
T_{ot} = 1.4×10^{8} °K
RADII (R_e)
DISTANCE ALONG TAIL AXIS (R_e)
ECCENTRICITY
0
25
50
500
1000
1500
0.0
0.5
1.0

Figure 13

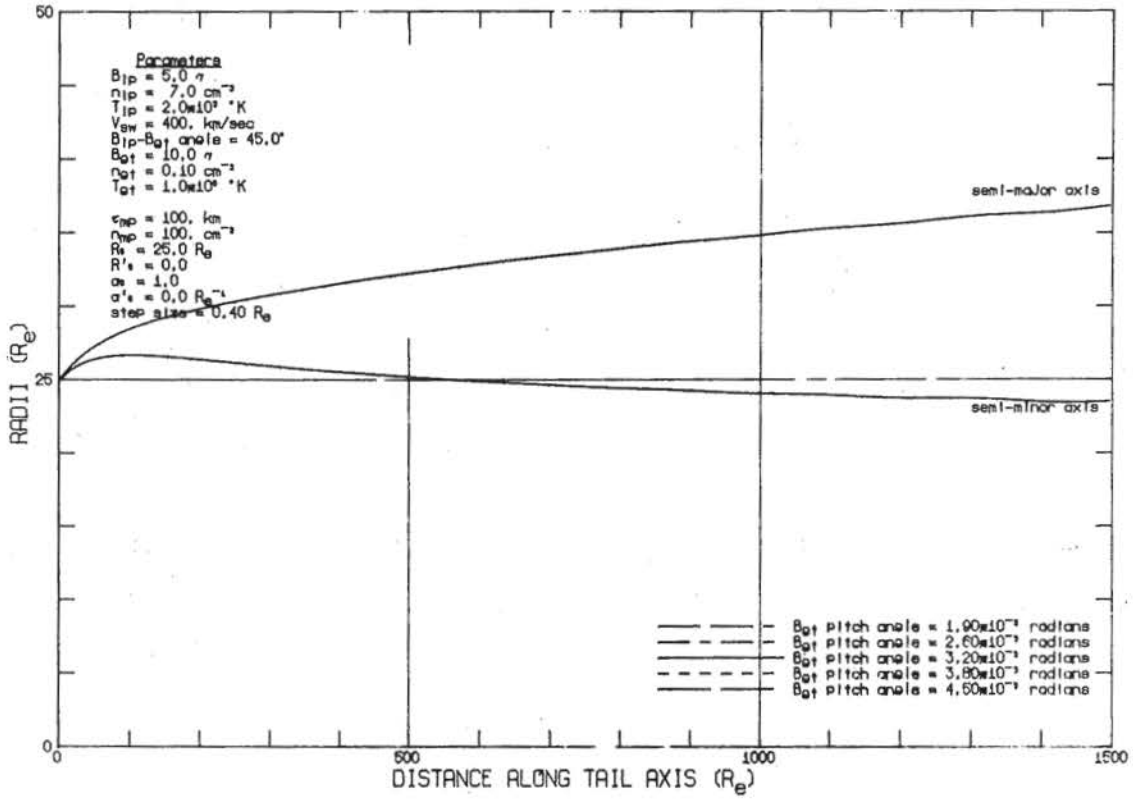
Parameters
B_{ip} = 5.0 γ
n_{ip} = 7.0 cm^{-3}
T_{ip} = 2.0x10^5 °K
V_{sw} = 400. km/sec
B_{ip}-B_{gt} angle = 45.0°
B_{gt} = 10.0 γ
n_{gt} = 0.10 cm^{-3}
T_{gt} = 1.0x10^6 °K
r_{mp} = 100. km
n_{mp} = 100. cm^{-3}
R_s = 25.0 R_e
R'_s = 0.0
α_s = 1.0
α'_s = 0.0 R_e^{-1}
step size = 0.40 R_e
semi-major axis
semi-minor axis
B_{gt} pitch angle = 1.90x10^{-1} radians
B_{gt} pitch angle = 2.60x10^{-1} radians
B_{gt} pitch angle = 3.20x10^{-1} radians
B_{gt} pitch angle = 3.80x10^{-1} radians
B_{gt} pitch angle = 4.50x10^{-1} radians
RADII (R_e)
50
25
0
0
500
1000
1500
DISTANCE ALONG TAIL AXIS (R_e)

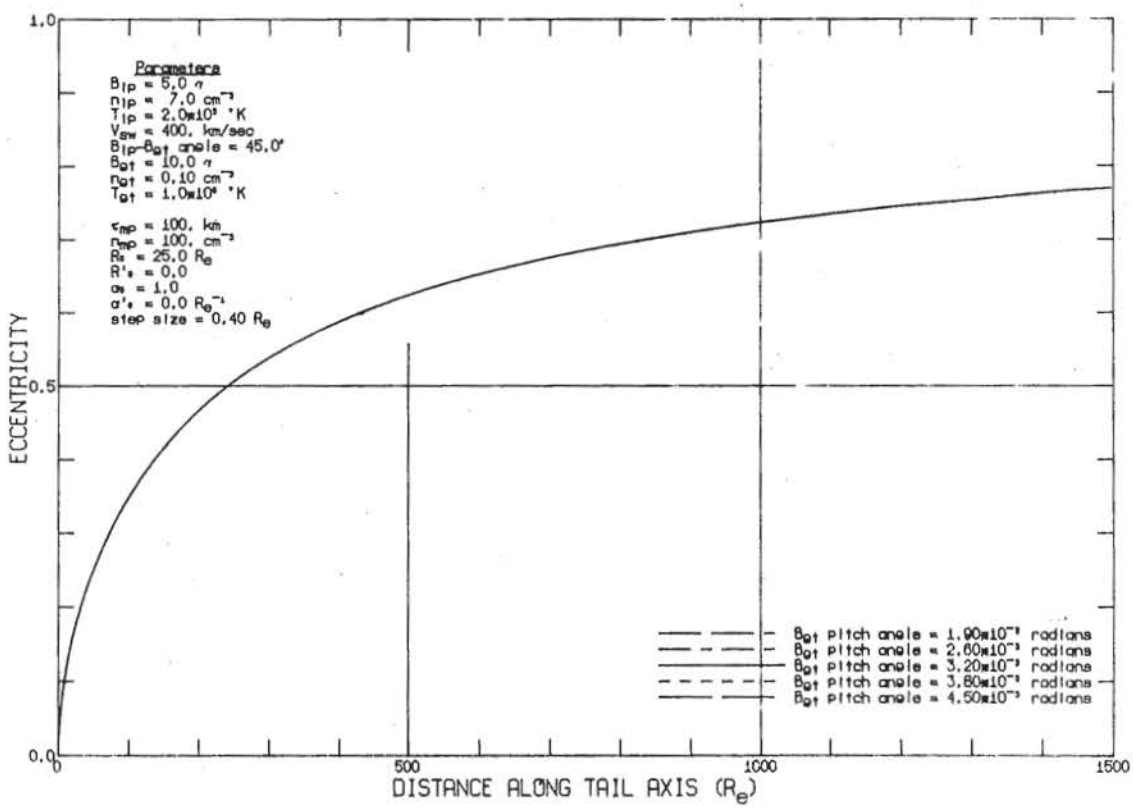
Parameters
B_{ip} = 5.0 γ
n_{ip} = 7.0 cm^{-3}
T_{ip} = 2.0x10^5 °K
V_{sw} = 400. km/sec
B_{ip}-B_{gt} angle = 45.0°
B_{gt} = 10.0 γ
n_{gt} = 0.10 cm^{-3}
T_{gt} = 1.0x10^6 °K
r_{mp} = 100. km
n_{mp} = 100. cm^{-3}
R_s = 25.0 R_e
R'_s = 0.0
α_s = 1.0
α'_s = 0.0 R_e^{-1}
step size = 0.40 R_e
B_{gt} pitch angle = 1.90x10^{-1} radians
B_{gt} pitch angle = 2.60x10^{-1} radians
B_{gt} pitch angle = 3.20x10^{-1} radians
B_{gt} pitch angle = 3.80x10^{-1} radians
B_{gt} pitch angle = 4.50x10^{-1} radians
ECCENTRICITY
1.0
0.5
0.0
0
500
1000
1500
DISTANCE ALONG TAIL AXIS (R_e)

Figure 14

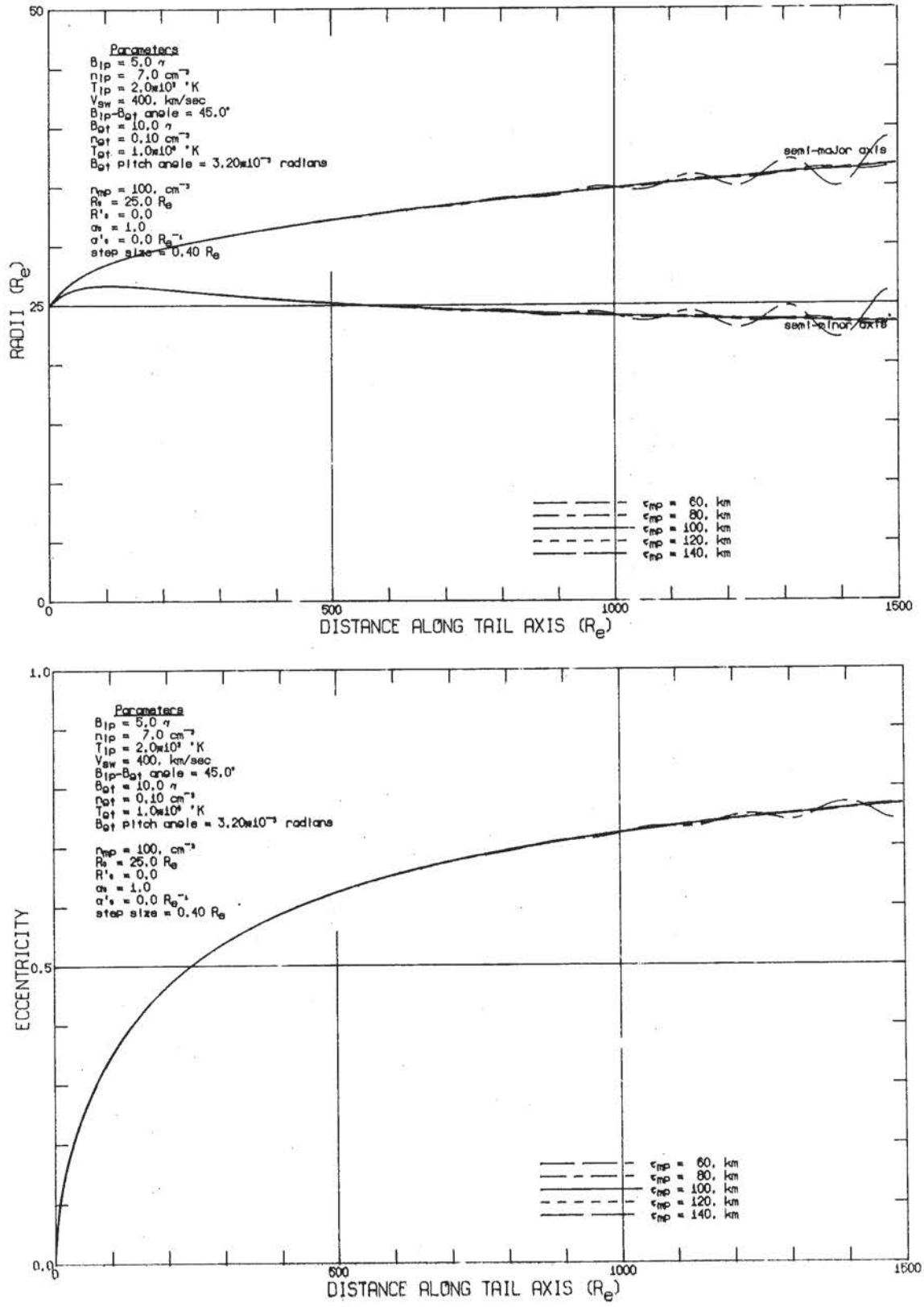
Parameters
B_{ip} = 5.0 γ
n_{ip} = 7.0 cm^{-3}
T_{ip} = 2.0×10⁵ °K
V_{sw} = 400. km/sec
B_{ip}-B_{ot} angle = 45.0°
B_{ot} = 10.0 γ
n_{ot} = 0.10 cm^{-3}
T_{ot} = 1.0×10⁶ °K
B_{ot} pitch angle = 3.20×10⁻³ radians
n_{mp} = 100. cm^{-3}
R_s = 25.0 R_e
R'$_s$ = 0.0
α_s = 1.0
α'_s = 0.0 R_e^{-1}
step size = 0.40 R_e
semi-major axis
semi-minor axis
r_{mp} = 60. km
r_{mp} = 80. km
r_{mp} = 100. km
r_{mp} = 120. km
r_{mp} = 140. km
RADII (R_e)
DISTANCE ALONG TAIL AXIS (R_e)
ECCENTRICITY
0
25
50
500
1000
1500
0.0
0.5
1.0

Figure 15

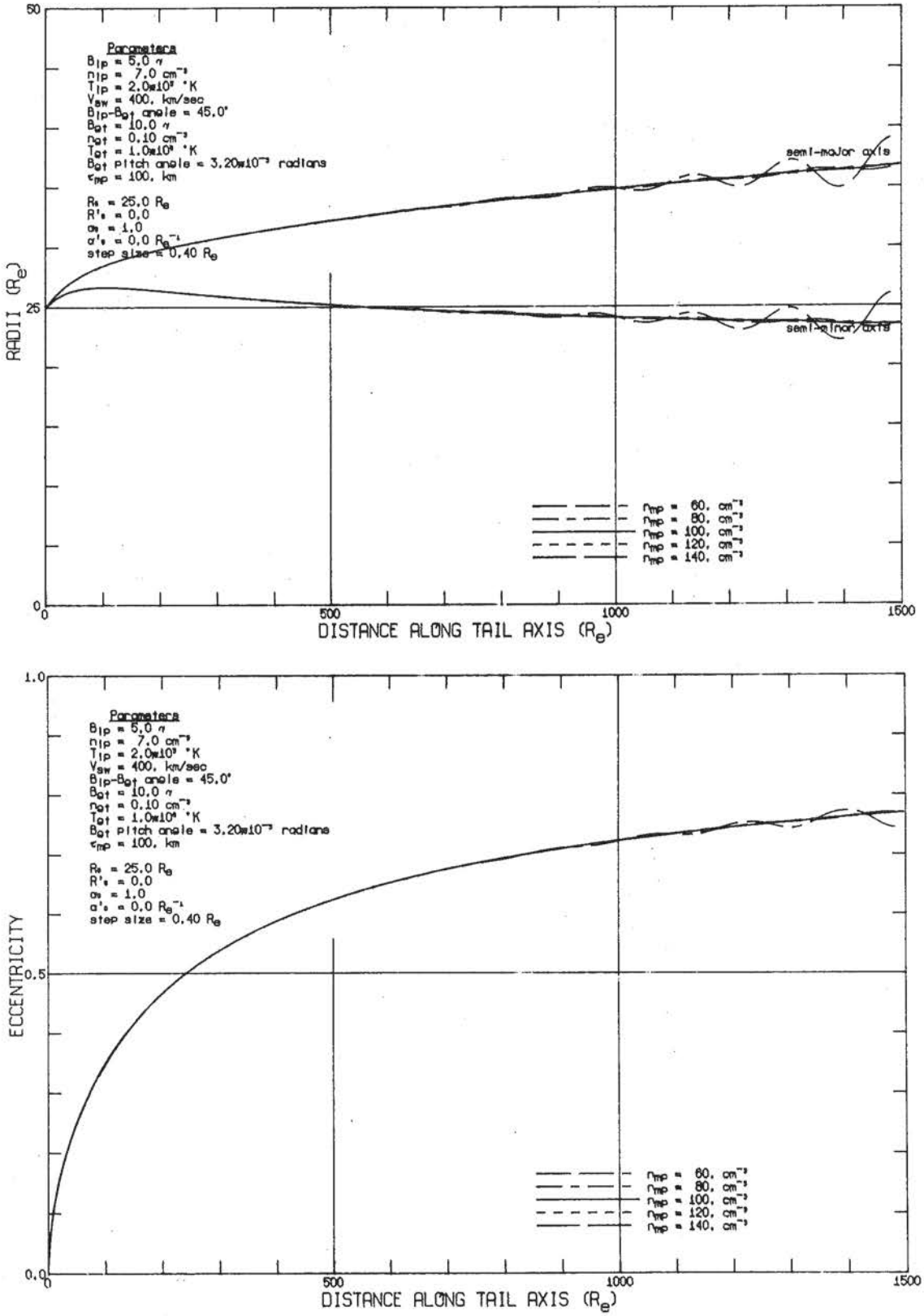
Parameters
B_{ip} = 5.0 γ
n_{ip} = 7.0 cm^{-3}
T_{ip} = 2.0×10^5 °K
V_{sw} = 400. km/sec
B_{ip}-B_{ot} angle = 45.0°
B_{ot} = 10.0 γ
n_{ot} = 0.10 cm^{-3}
T_{ot} = 1.0×10^6 °K
B_{ot} pitch angle = 3.20×10^{-3} radians
ϵ_{mp} = 100. km
R_s = 25.0 R_e
R'_s = 0.0
α_s = 1.0
α'_s = 0.0 R_e^{-1}
step size = 0.40 R_e
semi-major axis
semi-minor axis
n_{mp} = 60. cm^{-3}
n_{mp} = 80. cm^{-3}
n_{mp} = 100. cm^{-3}
n_{mp} = 120. cm^{-3}
n_{mp} = 140. cm^{-3}
RADII (R_e)
50
25
0
0
500
1000
1500
DISTANCE ALONG TAIL AXIS (R_e)
Parameters
B_{ip} = 5.0 γ
n_{ip} = 7.0 cm^{-3}
T_{ip} = 2.0×10^5 °K
V_{sw} = 400. km/sec
B_{ip}-B_{ot} angle = 45.0°
B_{ot} = 10.0 γ
n_{ot} = 0.10 cm^{-3}
T_{ot} = 1.0×10^6 °K
B_{ot} pitch angle = 3.20×10^{-3} radians
ϵ_{mp} = 100. km
R_s = 25.0 R_e
R'_s = 0.0
α_s = 1.0
α'_s = 0.0 R_e^{-1}
step size = 0.40 R_e
n_{mp} = 60. cm^{-3}
n_{mp} = 80. cm^{-3}
n_{mp} = 100. cm^{-3}
n_{mp} = 120. cm^{-3}
n_{mp} = 140. cm^{-3}
ECCENTRICITY
1.0
0.5
0.0
0
500
1000
1500
DISTANCE ALONG TAIL AXIS (R_e)

Figure 16

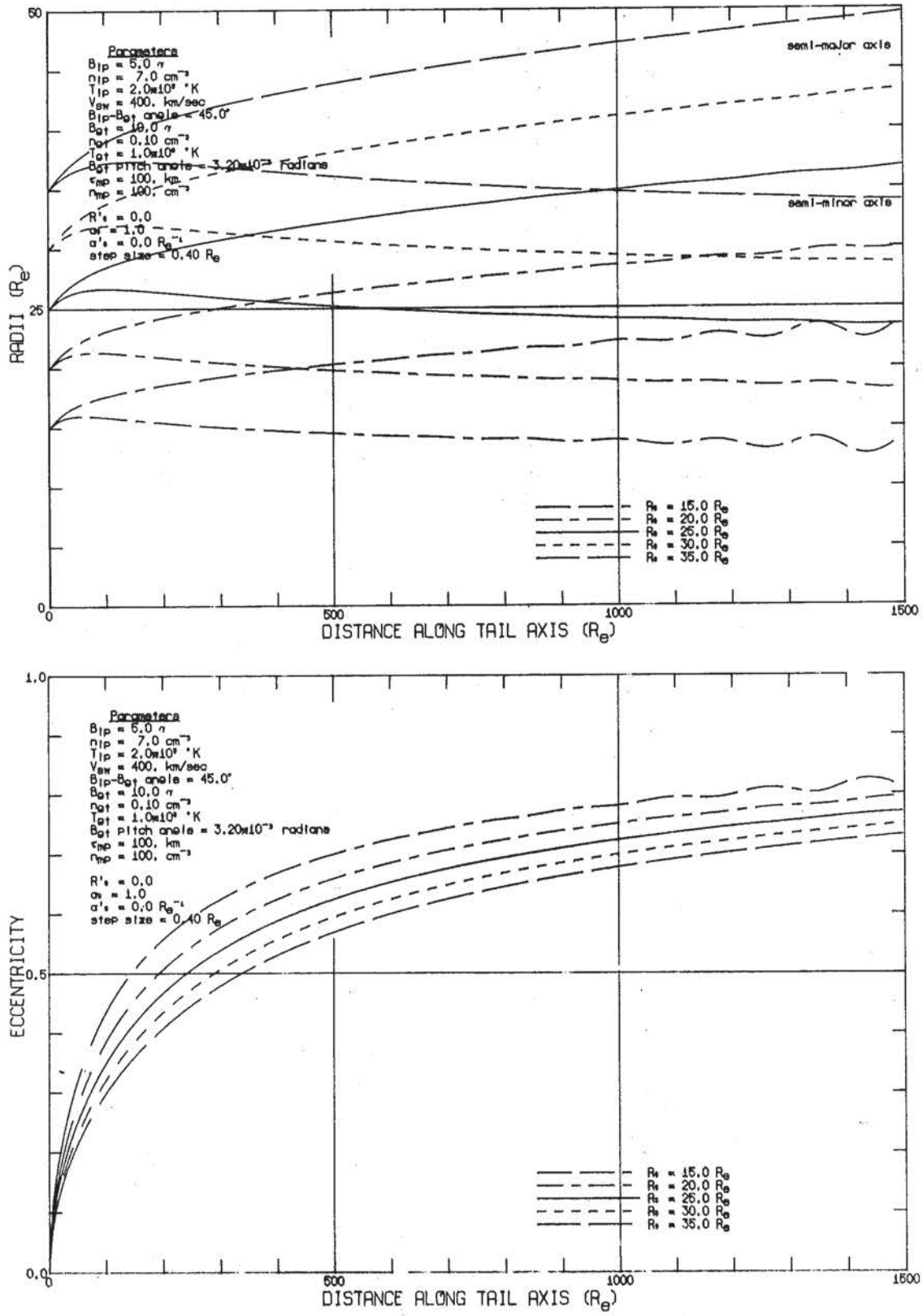
Parameters
B_{ip} = 5.0 γ
n_{ip} = 7.0 cm^{-3}
T_{ip} = 2.0×10^{6} °K
V_{sw} = 400. km/sec
B_{ip}-B_{ot} angle = 45.0°
B_{ot} = 10.0 γ
n_{ot} = 0.10 cm^{-3}
T_{ot} = 1.0×10^{8} °K
B_{ot} pitch angle = 3.20×10^{-3} radians
τ_{mp} = 100. km
n_{mp} = 100. cm^{-3}
R's = 0.0
α_s = 1.0
α'_s = 0.0 R_e^{-1}
step size = 0.40 R_e
semi-major axis
semi-minor axis
R_s = 15.0 R_e
R_s = 20.0 R_e
R_s = 25.0 R_e
R_s = 30.0 R_e
R_s = 35.0 R_e
RADII (R_e)
DISTANCE ALONG TAIL AXIS (R_e)
ECCENTRICITY
0
25
50
500
1000
1500
0.0
0.5
1.0

Figure 17

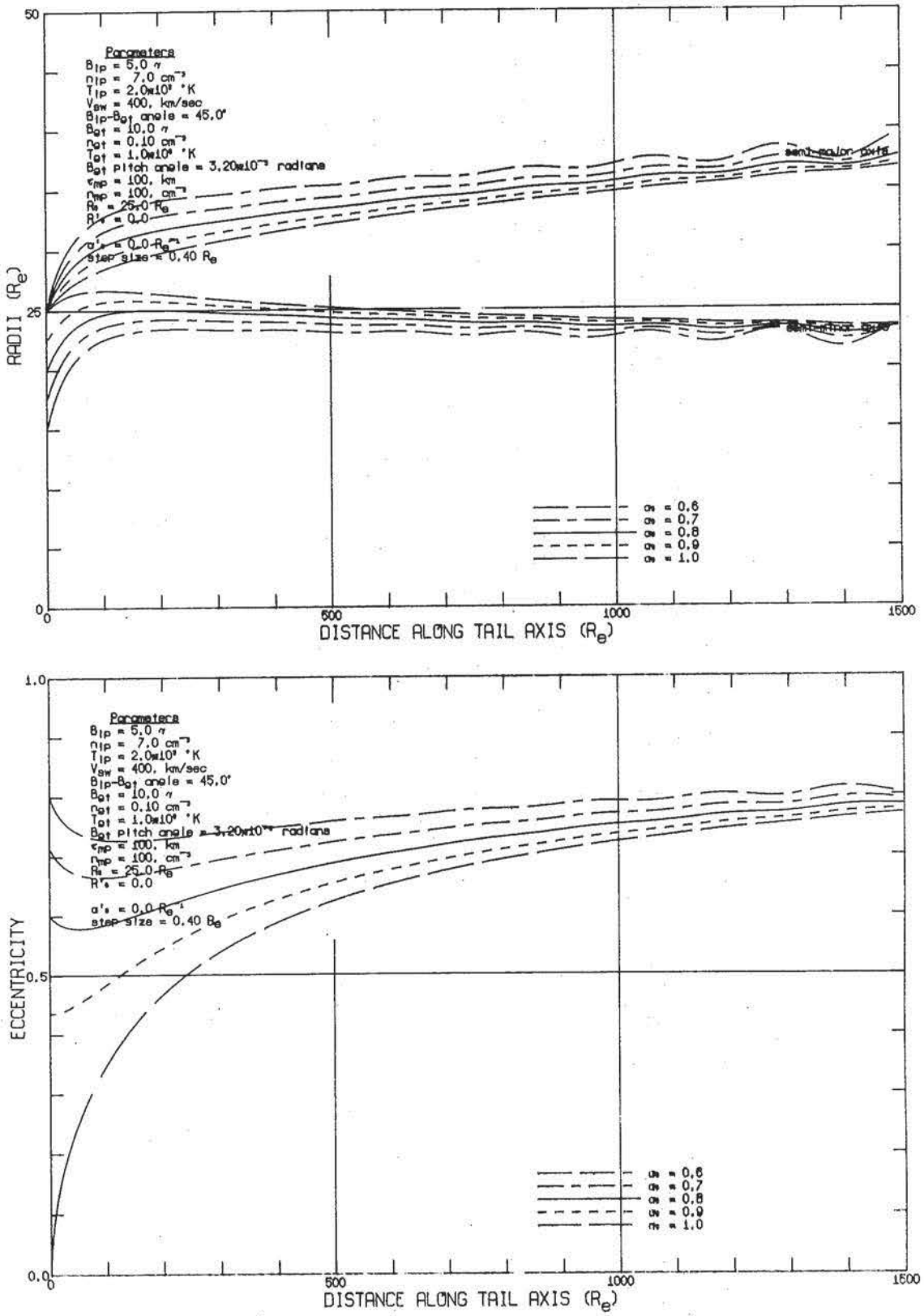
Parameters
B_{ip} = 5.0 γ
n_{ip} = 7.0 cm^{-3}
T_{ip} = 2.0×10^{5} °K
V_{sw} = 400. km/sec
B_{ip}-B_{at} angle = 45.0°
B_{at} = 10.0 γ
n_{at} = 0.10 cm^{-3}
T_{at} = 1.0×10^{6} °K
B_{at} pitch angle = 3.20×10^{-3} radians
r_{mp} = 100. km
n_{mp} = 100. cm^{-3}
R_s = 25.0 R_e
R'$_s$ = 0.0
a'$_s$ = 0.0 R_e^{-1}
step size = 0.40 R_e
semi-major axis
semi-minor axis
g = 0.6
g = 0.7
g = 0.8
g = 0.9
g = 1.0
RADII (R_e)
DISTANCE ALONG TAIL AXIS (R_e)
ECCENTRICITY
0
500
1000
1500
50
25
1.0
0.5
0.0

Figure 18

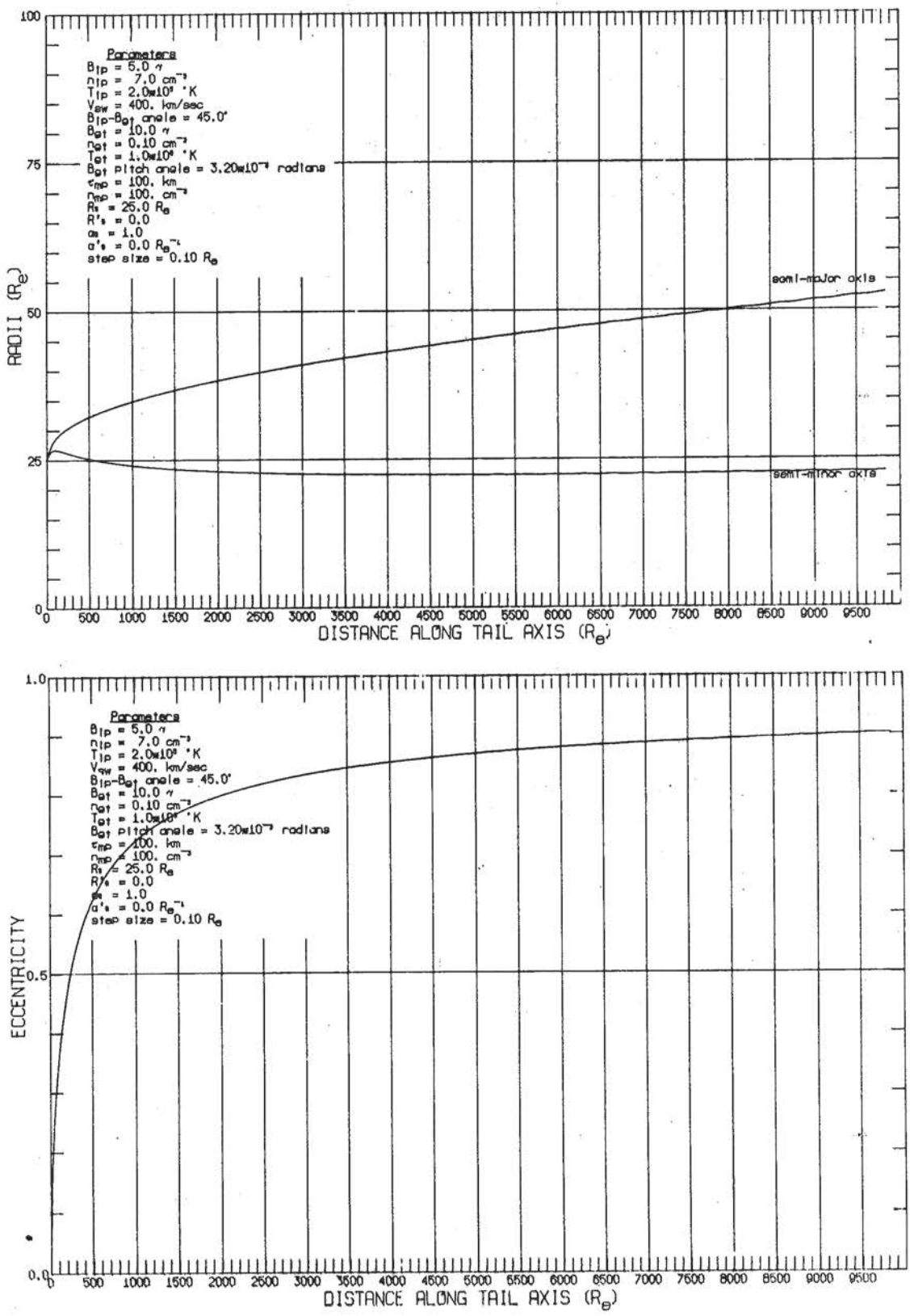
Parameters
B_{lp} = 5.0 γ
n_{lp} = 7.0 cm⁻³
T_{lp} = 2.0x10⁶ °K
V_{sw} = 400. km/sec
B_{lp}-B_{gt} angle = 45.0°
B_{gt} = 10.0 γ
n_{gt} = 0.10 cm⁻³
T_{gt} = 1.0x10⁸ °K
B_{gt} pitch angle = 3.20x10⁻³ radians
r_{mp} = 100. km
n_{mp} = 100. cm⁻³
R_s = 25.0 R_e
R'_s = 0.0
a_s = 1.0
a'_s = 0.0 R_e^{-1}
step size = 0.10 R_e
semi-major axis
semi-minor axis
RADII (R_e)
DISTANCE ALONG TAIL AXIS (R_e)
ECCENTRICITY
DISTANCE ALONG TAIL AXIS (R_e)

Figure 19

REFERENCES

Michel, F.C. and A. J. Dessler, "Diffusive Entry of Solar-Flare Particles into Geomagnetic Tail", J. Geophys. Res., 75, 6061 (1970).

Dessler, A.J. and R. D. Juday, "Configuration of Auroral Radiation in Space", Planetary Space Sci., 13, 63 (1965).

Landau, L.D. and E. M. Lifshitz, Fluid Mechanics, Addison-Wesley Publishing Company, Inc., Reading, Mass., 1959.

Stratton, J.A., Electromagnetic Theory, McGraw-Hill Book Co., Inc., New York, N.Y., 1941.